Atmos. Chem. Phys. Discuss., 10, 22219–22277, 2010
www.atmos-chem-phys-discuss.net/10/22219/2010/
doi:10.5194/acpd-10-22219-2010

Atmospheric Chemistry and Physics Discussions

Measurements of tropospheric HO_2 and RO_2 by oxygen dilution modulation and chemical ionization mass spectrometry

R. S. Hornbrook[1], **J. H. Crawford**[2], **G. D. Edwards**[1,*], **O. Goyea**[1,**], **R. L. Mauldin III**[1,3], **J. S. Olson**[2], **and C. A. Cantrell**[1]

[1]Atmospheric Chemistry Division, National Center for Atmospheric Research, 1850 Table Mesa Drive, P.O. Box 3000, Boulder, CO, USA
[2]Atmospheric Sciences Division, Langley Research Center, NASA, Hampton, VA, USA
[3]Department of Physics, 00014 University of Helsinki, Finland
[*]now at: Department of Chemistry, Eastern Michigan University, Ypsilanti, MI, USA
[**]now at: United States Patent and Trademark Office, Department of Commerce, Alexandria, VA, USA

Received: 2 September 2010 – Accepted: 8 September 2010
– Published: 28 September 2010

Correspondence to: R. S. Hornbrook (rsh@ucar.edu)

Published by Copernicus Publications on behalf of the European Geosciences Union.

Abstract

An improved method for the measurement of hydroperoxy radicals (HO_2) and organic peroxy radicals (RO_2, where R is any organic group) has been developed that combines two previous chemical conversion/chemical ionization mass spectrometry (CIMS) peroxy radical measurement techniques. Applicable to both ground-based and aircraft platforms, the method provides good separation between HO_2 and RO_2 and frequent measurement capability with observations of both HO_2 and $HO_2 + RO_2$ amounts each minute. This allows for analyses of measured $[HO_2]/[HO_2 + RO_2]$ ratios on timescales relevant to tropospheric photochemistry. By varying both [NO] and $[O_2]$ simultaneously in the chemical conversion region of the PeRCIMS (Peroxy Radical CIMS) inlet, the method exploits the changing conversion efficiency of RO_2 to HO_2 under different inlet $[NO]/[O_2]$ to selectively observe either primarily HO_2 or the sum of HO_2 and RO_2. Two modes of operation have been established for ambient measurements: in the first half of the minute, RO_2 radicals are measured at close to 100% efficiency along with HO_2 radicals (low $[NO]/[O_2] = 2.53 \times 10^{-5}$) and in the second half of the minute, HO_2 is detected while the majority of ambient RO_2 radicals are measured with approximately 15% efficiency (high $[NO]/[O_2] = 6.80 \times 10^{-4}$). The method has been tested extensively in the laboratory under various conditions and for a variety of organic peroxy radicals relevant to the atmosphere and the results of these tests are presented. The modified PeRCIMS instrument has been deployed successfully using the current measurement technique on a number of aircraft campaigns, including on the NSF/NCAR C-130 during the MIRAGE-Mex and NASA INTEX-B field campaigns in the spring of 2006. A brief comparison of the peroxy radical measurements during these campaigns to a photochemical box model confirms that the PeRCIMS is able to successfully separate and measure HO_2 and RO_2 under the majority of tropospheric conditions.

ACPD

10, 22219–22277, 2010

1 Introduction

Peroxy radicals, including hydroperoxy radicals (HO_2) and organic peroxy radicals (RO_2, where R is any organic group) are important tropospheric photochemical species having a critical role in tropospheric ozone formation, as a reservoir for hydroxyl radicals (OH), and the primary source of gas phase peroxides. Peroxy radicals are produced via reactions of OH with carbon monoxide and volatile organic compounds (VOCs). In air masses with low NO_x ($NO + NO_2$), the dominant sinks for peroxy radicals are via self- and cross reactions, forming peroxides and other species (Tyndall et al., 2001; Hasson et al., 2003; Calvert et al., 2008) Where NO_x concentrations are higher, peroxy radicals efficiently convert NO into NO_2, regenerating OH. The resulting NO_2 can be photolyzed to generate O_3. At very high NO_x, production of HNO_3 from the reaction of OH with NO_2 dominates.

The presently-available techniques used for observing RO_2 do not provide speciated measurements of individual RO_2 but rather a sum of RO_2 (Cantrell et al., 2003a, b, c; Green et al., 2006; Ren et al., 2006; Fuchs et al., 2008). Nevertheless, observations of organic peroxy and hydroperoxy radicals have been shown to be valuable components in understanding and modeling tropospheric photochemistry. Separate observations of $[HO_2]$ and $[HO_2 + RO_2]$ under photochemical timescales can improve our understanding of atmospheric processes involving VOCs and NO_x and the partitioning that occurs between OH and HO_2 and between the hydro- and organic peroxy radical forms.

The method presented here builds on the previous work of this research group using the Peroxy Radical Chemical Ionization Mass Spectrometry (PeRCIMS) inlet (Edwards et al., 2003) by adding a dilution step similar to that described by Hanke et al. (2002). In all three techniques, $[HO_2]$ and $[HO_2 + RO_2]$ are measured independently by exploiting the competing chemistry that converts alkoxy (RO) radicals, formed in reactions of RO_2 with added NO in the inlet, into either HO_2 or alkyl nitrites via the following:

$$RO_2 + NO \rightarrow RO + NO_2 \quad \text{(R1)}$$

$$RO + NO + M \rightarrow RONO + M \quad \text{(R2)}$$

ACPD
10, 22219–22277, 2010

$$RO + O_2 \rightarrow R'O + HO_2 \quad \text{(R3)}$$

$$RO_2 + NO + M \rightarrow RONO_2 + M \quad \text{(R4)}$$

Here, Reaction (R3) requires that the RO radical has available α-hydrogen atoms that can be abstracted. For inlet conditions $k_3[O_2] > k_2[NO][M]$, there is increased likelihood for alkoxy radicals to react with O_2 to generate HO_2. Similarly, where $k_3[O_2] < k_2[NO][M]$, RO is more likely to form an alkyl nitrite via (R2). For some RO_2 radicals, there is also the possibility of formation of the alkyl nitrate via (R4) in competition with (R1), generally increasing in importance as the size of the R group increases. This RO_2 separation chemistry is shown in Scheme 1, along with an additional reaction pathway that will be discussed in Sect. 3.2.3.

Both ambient HO_2 radicals and HO_2 radicals formed in Reaction (R3) are converted into H_2SO_4 in the inlet through reactions with added NO and SO_2 via:

$$HO_2 + NO \rightarrow OH + NO_2 \quad \text{(R5)}$$

$$OH + SO_2 + M \rightarrow HSO_3 + M \quad \text{(R6)}$$

$$HSO_3 + O_2 \rightarrow HO_2 + SO_3 \quad \text{(R7)}$$

$$SO_3 + 2H_2O \rightarrow\rightarrow H_2SO_4 + H_2O \quad \text{(R8)}$$

$$OH + NO + M \rightarrow HONO + M \quad \text{(R9)}$$

The formation of HSO_3 in (R6) leads to HO_2 being recycled in (R7), but this cycle is terminated by (R9). Therefore, the residence time in the neutral chemistry region and the ratio of $[SO_2]/[NO]$ determines the competing chemistry of OH reactions with SO_2 and NO (R6 and R9), and thus the sulfuric acid yield, $\Delta[H_2SO_4]/[HO_2]_o$, from (R5–R8). A summary of the HO_2 conversion chemistry is shown in Scheme 2.

The method described by Edwards et al. (2003) involves varying [NO] in the chemical conversion region of the PeRCIMS inlet to either enhance or reduce the rate of (R2)

ACPD
10, 22219–22277, 2010

and likewise the measurement sensitivity to organic peroxy radicals. The concentration of NO in the inlet is changed by adding either pure NO or a 3000 ppmV (parts per million by volume) mixture of NO in N_2 to the front injector of the inlet. To maintain a constant chain length of $\Delta[H_2SO_4]/[HO_2]_o$, inlet $[SO_2]$ is simultaneously adjusted by adding either pure SO_2 gas or a 1% mixture of SO_2 in N_2 to the front injector gas mixture. A serious drawback to this method is the time required to switch from HO_2 measurement to $HO_2 + RO_2$ measurement: on the order of 30 min to allow adequate time for the pure reagent gases to be flushed from the inlet. Using this method, the conversion efficiency of RO_2 into HO_2 (α_{RO_2}) is reported to be 0.10–0.15 using pure reagent gases and 0.80–0.90 using dilute reagent gas mixtures, giving an approximate sixfold separation between HO_2 and $HO_2 + RO_2$, but under timescales that are long in comparison to photochemistry and not ideal for aircraft measurements.

Using an inlet similar to the PeRCIMS inlet with the same conversion chemistry, Hanke et al. (2002) describe a CIMS method in which RO_2 is selectively measured by adjusting the O_2 concentration in the chemical conversion region to either enhance or reduce the rate of (R3). This is done by diluting the sample flow by 75% or more with either O_2 or N_2. A constant sample flow is maintained while the $[NO]/[O_2]$ ratio in the inlet is increased or decreased. The authors reported α_{RO_2} values of 0.25–0.30 with N_2 dilution (HO_2 mode), and 0.90 with O_2 dilution ($HO_2 + RO_2$ mode), with measurements of both modes made approximately once per minute. While the reported one-minute measurement cycle is more appropriate for timescales relevant to photochemistry and airborne measurements, the separation between HO_2 and $HO_2 + RO_2$ is weaker in comparison to the method described by Edwards and colleagues. Additionally, there is an inherent loss in sensitivity caused by diluting the ambient sample to one quarter or less of the sample flow.

The method we present here is a combination of the two methods described above in which both [NO] and $[O_2]$ are modulated in the inlet to generate a low $[NO]/[O_2]$ measurement mode and a high $[NO]/[O_2]$ measurement mode. By varying the inlet $[O_2]$, the requirement for pure NO and SO_2 reagent gases is eliminated. Likewise, by adjust-

ACPD
10, 22219–22277, 2010

ing the NO mixture flow rate, good separation can be achieved with only 50% dilution of the sample air. This enables independent [HO_2] and [$HO_2 + RO_2$] observations to be made each minute and simultaneously provides better measurement sensitivity and separation than with dilution alone. Although two measurement modes have been established for observations of ambient peroxy radicals via the new method, the modified PeRCIMS inlet has been tested extensively in the laboratory under a wide range of [NO]/[O_2] conditions to characterize the oxygen dilution modulation method under a variety of conditions and for a large selection of common organic peroxy radicals.

2 Experimental

2.1 Principles of operation

Shown in Fig. 1, the modified PeRCIMS instrument utilizes a technique in which ambient HO_2 and RO_2 are chemically converted to HSO_4^- ions that are then detected quantitatively by mass spectrometry. With the exception of the diluent region, the basic components of the instrument are similar to that described by Edwards et al. (2003), and thus only a summary is presented here.

2.2 Dilution

The primary modification to the instrumentation is the addition of a dilution region to the intake region of the inlet (Fig. 1, inset). Sample air containing peroxy radicals is drawn through a 2.7-mm diameter orifice into the dilution region of the PeRCIMS inlet where either N_2 or O_2 (UHP, United States Welding) is added. For ambient peroxy radical observations, two measurement modes have been established and the details for these are listed in Table 1. In the $HO_2 + RO_2$ mode, sampled air is diluted by half with O_2, and in the HO_2 mode, sampled air is diluted by half with N_2. With ambient air at standard pressure and the internal inlet pressure controlled at 150 Torr, the flow of gas

ACPD
10, 22219–22277, 2010

from the dilution region of the inlet into the neutral chemistry region is 2.32 standard liters per minute (SLPM). Thus, to generate a 1:1 ratio of diluent to sample air, diluent O_2 and N_2 flow rates are controlled at 1.16 SLPM at sea level and adjusted to maintain a 1:1 ratio of diluent to sampled air for measurements at lower ambient pressures. Diluent gas switching is computer controlled using two low-volume three-way valves (Clippard) to maintain a constant flow of gas into the dilution region and to minimize pressure pulses in the diluent lines.

2.3 Inlet conversion chemistry

The mixture of sampled air and diluent is drawn from the dilution region through a 0.50-mm diameter orifice into the neutral chemistry region of the inlet, controlled at a constant pressure of 150 Torr by a scroll pump (Air Squared) and a pressure controller (MKS 640). Two reagent mixtures, 1.5% NO in N_2 and 4.0% SO_2 in N_2 (made in house using pure NO and SO_2 gases and UHP N_2) are added via the front injector at computer-controlled flow rates to generate NO mixing ratios of 15.0 and 67.5 ppmV and SO_2 mixing ratios of 400 and 1800 ppmV for the $HO_2 + RO_2$ and HO_2 modes, respectively.

In both modes, HO_2 radicals are chemically converted via Reactions (R5–R8) into gas phase H_2SO_4 with a $\Delta[H_2SO_4]/[HO_2]_o$ yield of 5.5. As described by Edwards et al. (2003), ambient OH radicals are measured alongside peroxy radicals in the PeRCIMS inlet. However, because ambient $[HO_2]/[OH]$ ratios are typically 50–100, the impact of OH on peroxy radical signals is insignificant given that peroxy radical measurement uncertainties are generally on the order of ±30%.

The conversion chemistry involved in the measurement of organic peroxy radicals by CIMS was described by Edwards and colleagues as being only slightly more complex than the measurement of HO_2, involving an initial conversion of RO_2 radicals with available α-hydrogen atoms to HO_2 via Reaction (R1) and (R3). With inlet conditions at a reduced pressure and relatively low [NO] such that $k_3[O_2] > k_2[NO][M]$, alkoxy radicals formed in Reaction (R1) will form HO_2 radicals which are then converted to

ACPD
10, 22219–22277, 2010

H_2SO_4 in the same manner as ambient HO_2. From extensive characterization experiments on the modified PeRCIMS inlet using a number of different RO_2 precursors at $[NO]/[O_2] < 1 \times 10^{-5}$, we have determined that there is an additional reaction pathway by which organic peroxy radicals are converted into H_2SO_4 in the PeRCIMS inlet. We will explore the inlet chemistry further in the discussion section.

2.4 Background measurement

Ambient H_2SO_4 and other chemical artifacts that react with SO_2 in the inlet to form H_2SO_4 add to the peroxy radical signal measurement, and thus each peroxy radical measurement in each mode is accompanied by a background measurement. To quantify the background, the SO_2 mixture added to the front injector during the signal measurement is redirected to the rear injector of the neutral chemistry region (see Fig. 1). The inlet chemistry proceeds such that OH radicals formed in (R5) react with NO to form HONO via (R9) prior to encountering SO_2, preventing the conversion of ambient peroxy radicals into H_2SO_4. The SO_2 mixture is directed to either the front or rear injector by a low-volume computer-controlled 3-way valve (Clippard). To maintain constant and balanced flows through the injectors for the entire measurement cycle for both modes, additional quantities of N_2 gas are added to the front and rear injectors. For typical operation, the duration of the background measurement is equal to the duration of the signal measurement. The actual peroxy radical concentration for each measurement mode is determined using the difference in the signal and background measurements.

2.5 Ion chemistry

Immediately following the neutral chemistry region of the inlet is the ion chemistry region where a fraction of the gas-phase H_2SO_4 molecules is converted into HSO_4^- ions via a proton-transfer reaction with NO_3^- ions and its clusters, similar to the reaction

ACPD
10, 22219–22277, 2010

scheme described by Tanner and Eisele (1995):

$$NO_3^- + H_2SO_4 \rightarrow HNO_3 + HSO_4^- . \quad \text{(R10)}$$

A mixture of air, nitric acid vapor and NO is added to the inlet at the end of the neutral chemistry region to provide a sheath flow within the ion chemistry region. This sheath mixture includes 2.32 SLPM of ambient air that has passed through a chemical scrubber to remove trace SO_2, as well as ~1.5 sccm (standard cubic centimeters per minute) of N_2 that has passed through the headspace of a vial containing liquid concentrated HNO_3 and ~5 sccm of the 1.5% NO in N_2 mixture. NO_3^- ions are produced as the HNO_3 vapor in the sheath flow is ionized by O_2^- and other more primary products generated by the radioactive source (^{241}Am). The NO added to the sheath air helps to lower the background by reacting with OH and other radicals produced by the source emission.

2.6 Ion detection

At the rear of the ion region, HSO_4^- ions are directed through a 0.2-mm diameter pinhole by a series of ion lenses located throughout the inlet and inside the vacuum system, along with other negatively-charged ions (i.e. NO_3^- and clusters of NO_3^- or HSO_4^- with neutral species). An N_2 buffer flow (200 sccm), immediately before the pinhole and greater than the flow into the pinhole, serves to prevent oxygen and other neutral gases from entering the vacuum system, while allowing ions, with the help of an electric field, to pass through while also reducing H_2O clustered with the ions.

For different applications or platforms, the PeRCIMS inlet has been affixed to a number of different vacuum systems, but the primary components in these vacuum systems are similar. Depending on the diameter and volume of the vacuum system, two or three turbomolecular pumps (Varian V550, Varian V301, Balzer-Pfeiffer TCP-380), mounted orthogonally to the ion stream and backed by a scroll pump (Air Squared, Synergy or Varian) are used to pump the vacuum system to pressures of 4×10^{-4} Pa or less. Immediately behind the pinhole is a collision dissociation chamber (CDC) which accelerates and aids in the dissociation of ion clusters, leaving primarily NO_3^- and HSO_4^-

ACPD
10, 22219–22277, 2010

ions. The CDC region is kept at a constant a pressure, ideally ~10 Pa, determined by the diameter of the orifice at the rear of the CDC, typically between 6 and 10 mm. After passing through the CDC, ions are guided further into the vacuum system either by a series of ion lenses or by an octopole ion guide assembly mounted immediately after the CDC, and are then mass-selected by a quadrupole mass filter with additional ion lenses before and after the quadrupoles. At the rear of the vacuum system, the ions selected by the mass filter are detected by a channel electron multiplier (Ceramax, K&M Electronics) biased in the negative ion pulse counting mode.

The ratio of the NO_3^- and HSO_4^- counting frequencies (counts/s) is proportional to the peroxy radical signal S according to:

$$S = \frac{(f_{HSO_4^-,\text{signal}}) - (f_{HSO_4^-,\text{background}})}{(f_{NO_3^-}) - (f_{\text{electronic noise}})} \quad (1)$$

where $f_{HSO_4^-,\text{signal}}$ and $f_{HSO_4^-,\text{background}}$ are the HSO_4^- counting frequencies when the SO_2 mixture is directed through the front and rear injectors, respectively, and $f_{\text{electronic noise}}$ is the counting frequency of a region of the mass spectrum where there are not typically ions present, typically *m/z* 20 or 70. Generally, $f_{\text{electronic noise}} \ll f_{NO_3^-}$, and thus this correction is only minor and the electronic noise measurement serves to confirm that there is not significant electronic noise present in the system.

2.7 Calibration

In a quartz calibration cell positioned in front of the inlet (Fig. 2), H_2O molecules are photolyzed by a low pressure Hg lamp (UVP, Jelight or Hamamatsu) with a quartz envelope emitting in the UV range (primarily at 184.9 and 253.7 nm) via:

$$H_2O_{(g)} + h\nu(184.9\text{ nm}) \rightarrow OH + H \quad (R11)$$

$$H + O_2 + M \rightarrow HO_2 + M. \quad (R12)$$

ACPD
10, 22219–22277, 2010

Air at a desired absolute humidity is generated by combining flows of dry synthetic air (US Welding, Hydrocarbon Free, total hydrocarbons ≤0.1 ppm) with synthetic air that has been saturated by passing through a 303-K temperature-controlled vessel containing PTFE spheres (Hoover Precision Products, Inc.; 1/4-in. diameter) wetted with deionized water. The humidity of the air mixture is monitored continually by directing 100 sccm of the total air mixture flow (5–20 SLPM) through a hygrometer (DewPrime III, Edgetech).

Radical production is controlled by varying the amount of radiation passing through the cell and the water vapor mixing ratio of the synthetic air. The amount of radiation in the calibration cell can be controlled by adjusting the distance between the lamp and the cell or by inserting slits of differing widths in the path of the radiation. Both of these properties could be adjusted on the previous calibration cell assembly (shown by Edwards et al., 2003), but only the slit width can be adjusted on the current calibration assembly (Fig. 2). Radical concentrations similar to those found in the atmosphere and greater are generated using this method. From Cantrell et al. (1997a, b), the yield of HO_2 radicals from the photolysis of water can be determined using

$$[HO_2] = (It)\sigma_{H_2O}\phi_{H_2O}[H_2O] \quad (2)$$

where σ_{H_2O} is the absorption cross section of water vapor (i.e. 7.22×10^{-20} cm^2 molecule^{-1}) and ϕ_{H_2O} is the photolysis quantum yield (assumed to be unity) at 184.9 nm. The quantity It is the product of the lamp flux and the photolysis time, and is determined for each calibration cell assembly in separate N_2O actinometry experiments for specific slits and flow rates through the calibration cell.

To generate a fixed hydroperoxy radical concentration, H_2 (United States Welding or National Specialty Gases) is added to the humidified air flow. OH formed in (R11) reacts with H_2 to generate HO_2 according to

$$H_2 + OH \rightarrow H_2O + H \quad (R13)$$

$$H + O_2(+M) \rightarrow HO_2(+M). \quad (R14)$$

ACPD
10, 22219–22277, 2010

Thus, the total [HO_2] produced is $2(It)\sigma_{H_2O}\phi_{H_2O}[H_2O]$. In the absence of added H_2, the OH will react with trace gases in the synthetic air and will create an unknown mixture of hydroperoxy and organic peroxy radicals.

3 Instrument characterization

A number of tests have been performed on the PeRCIMS instrument to characterize the inlet chemistry and to establish the ambient measurement modes for optimum sensitivity and separation of HO_2 and $HO_2 + RO_2$. These characterizations were made using both the previous and current calibration cell assemblies described above for absolute calibrations. In general, H_2 and CH_4 (or another RO_2 precursor) are added individually to the humidified air that passes through the calibration cell, with the output of the cell directly in front of the PeRCIMS inlet. Generating organic peroxy radicals using H_2O photolysis is preferential to using Cl atom + precursor reactions as OH chemistry produces RO_2 species more commonly encountered in the atmosphere. As with the absolute calibration, OH radicals formed via (R11) react with H_2 to generate a second HO_2 for each water molecule photolyzed, according to (R13) and (R14). Adding CH_4 in place of H_2 generates a methyl peroxy radical according to:

$$CH_4 + OH \rightarrow H_2O + CH_3 \quad \text{(R15)}$$

$$CH_3 + O_2(+M) \rightarrow CH_3O_2(+M), \quad \text{(R16)}$$

resulting in equal parts HO_2 and CH_3O_2 radicals. The background-corrected signals of the peroxy radicals generated from the addition of the two precursors, S_{CH_4} and S_{H_2}, under otherwise identical inlet conditions, are used to determine $\alpha_{CH_3O_2}$ (the conversion efficiency or measurement sensitivity to CH_3O_2 in comparison to HO_2) according to:

$$\alpha_{CH_3O_2} = 2 \times \left(\frac{S_{CH_4,ave}}{S_{H_2,ave}} \right) - 1 \quad (3)$$

ACPD
10, 22219–22277, 2010

or, in general for any organic peroxy radical precursor, RH:

$$\alpha_{RO_2} = 2 \times \left(\frac{S_{RH,ave}}{S_{H_2,ave}} \right) - 1. \quad (4)$$

Determinations of α_{RO_2} have been made for a number of RO_2 precursors over a wide range of [NO]/[O_2] values between 10^{-2} and 10^{-6}. Each α_{RO_2} determination requires a peroxy radical measurement with H_2 added to the humidified synthetic air, and a peroxy radical measurement with CH_4 or other RO_2 precursor added. Reported α_{RO_2} values were determined using $S_{RH,ave}$ and $S_{H_2,ave}$, the respective means of approximately four consecutive individual S_{RH} measurements and S_{H_2} measurements, such that all measurements are made within ~10 min.

To characterize the inlet chemistry and establish the two ambient observation modes, a broad set of operating conditions have been tested with a variety of peroxy radical precursors and concentrations and are described in the following sections. To ensure ideal conditions for each α_{RO_2} determination, individual calibration parameters were investigated to determine ideal operating ranges for the total flow rate through the calibration cell and the concentrations of the radical precursors. The results of these tests are discussed in the following section. Using conditions that fell within these ideal operating parameters, $\alpha_{CH_3O_2}$ has been measured more than 1000 times over a broad range of inlet [NO] and [NO]/[O_2]. The results of these measurements are shown in Fig. 3. With inlet [NO]<2 ppmV, there is less $\alpha_{CH_3O_2}$ dependence on inlet [O_2], but for inlet [NO]>2 ppmV, the concentration of O_2 in the inlet plays a more important role in determining $\alpha_{CH_3O_2}$, and the ratio of [NO]/[O_2] is key. The $\alpha_{CH_3O_2}$ data were binned by [NO]/[O_2] value, and the mean $\alpha_{CH_3O_2}$ values for each bin are shown in Fig. 3a and listed in Table 2 along with the mean $\alpha_{CH_3O_2}$ values for the two ambient measurement modes.

ACPD
10, 22219–22277, 2010

3.1 Calibration parameter experiments

3.1.1 Total flow rate through the calibration cell

The concentration of radicals formed in the calibration cell depends on both the total flow rate of the humidified air mixture through the cell and the amount of irradiation with which the water vapor in the air is exposed, *It* (Eq. 3). The ideal total flow rate through the calibration cell was determined for three lamp intensities (generated with the lamp at three different distances from the cell using the old calibration cell apparatus) at five different total calibration cell flow rates. For each flow rate, the relative flow rates of saturated and dry air were held constant at 1:10, or ~9.1% relative humidity at room temperature. For all measurements reported for this test the inlet [NO]/[O_2] was 1.29×10^{-5} with 1.0 SLPM of O_2 added to the dilution region, and 10 sccm each CH_4 and H_2. A minimum of two $\alpha_{CH_3O_2}$ measurements (8 individual measurements with each precursor) were made for each lamp distance at each total air flow rate. A summary of the results of the test is shown in Table 3.

The measured $\alpha_{CH_3O_2}$ values indicate that with a specified concentration of water, a minimum flow rate through the calibration cell is necessary, as it is otherwise possible to generate too many peroxy radicals to be quantitatively converted to H_2SO_4 without requiring a correction for NO_3^- depletion in the inlet. With a constant water vapor mixing ratio, a slower total flow rate results in a longer exposure time to irradiation in the calibration cell and thus a larger fixed radical concentration. To avoid needing to correct for NO_3^- depletion, calibrations made at a minimum flow rate of approximately 3 SLPM of synthetic air at a relative humidity of approximately 10% at room temperature through the calibration cell is ideal. A standard operating procedure using 5 SLPM of 10% humidified air has been adopted based on these results.

ACPD
10, 22219–22277, 2010

3.1.2 Water vapor mixing ratio

The modified PeRCIMS inlet has also been tested using a range of water vapor mixing ratios in the calibration cell air mixture to establish whether or not there is stability across a range of humidities by measuring $\alpha_{CH_3O_2}$ at the ambient mode conditions. The total flow through the calibration cell was held constant at 5 SLPM, but the relative flows of saturated air and dry synthetic air were adjusted to generate humidified fractions ranging from 5 to 40% of the total flow. During these measurements, alternating diluent N_2 and O_2 were added to generate a 1:1 ratio with the sample air from the calibration cell, and 10 sccm of alternating CH_4 and H_2 were added to the humidified air. The resulting $\alpha_{CH_3O_2}$ values, as well as the error-weighted mean $\alpha_{CH_3O_2}$ value for each humidity studied are shown in Fig. 4.

From the water vapor calibration test, $\alpha_{CH_3O_2}$ appears to be independent of the humidity of the calibration air mixture over a range of saturations from 5 to 25%. Based on the results from this test, we have confidence in other experiments that were performed under similar conditions with 10% saturated air in the calibration cell. There is, however, a lower limit on the absolute water vapor mixing ratio in the inlet for conversion of ambient peroxy radicals into H_2SO_4. This is based on (R8), in which the rate of the conversion of SO_3 into H_2SO_4 is proportional to the square of the water mixing ratio in the inlet. We have calculated the lower limit for water content over a range of atmospheric relative humidities and temperatures, and have determined that the PeRCIMS is sufficiently sensitive (i.e. the calibration factors are stable with regards to the measurement of peroxy radicals) under the majority of tropospheric conditions. However, because the sampled air is drawn from ambient pressure into a low pressure region and being diluted 1:1 with dry N_2 or O_2, there are possible ambient conditions in which the measurement sensitivity could be lowered. This typically involves air masses that are very dry and cold, i.e. measurements at low altitudes in dry arctic regions. Figure 5 shows the calculated dependence on ambient pressure and temperature for a series of minimum relative humidities at which peroxy radicals can be measured without any

ACPD
10, 22219–22277, 2010

modifications to the sampling procedure. For field studies in which conditions are below these minimum relative humidity curves, we have developed a method in which a fraction of the diluents (N_2 and O_2) are humidified to add sufficient water vapor to the inlet.

3.1.3 Peroxy radial precursor concentration

The calibration and α_{RO_2} characterizations of the peroxy radical measurement rely on the OH-chemistry of CH_4 and H_2 in the calibration cell to generate reproducible mixing ratios of HO_2 and CH_3O_2. When insufficient amounts of CH_4 or H_2 are added to the humidified air, trace contaminants in the air or other reagent gases can react with OH in place of CH_4 and H_2, generating unknown [CH_3O_2], [HO_2] or other radicals. With excessively high CH_4 or H_2 mixing ratios, the conversion of CH_3O_2 and HO_2 to H_2SO_4 in the inlet will not reach completion due to competition with SO_2 for OH. To determine the ideal concentration range of peroxy radical precursors in the calibration cell flow, two tests were performed using a range of CH_4 and H_2 flow rates added to the total calibration flow.

In the first test, $\alpha_{CH_3O_2}$ was determined at three [NO]/[O_2] ratios (9.30×10^{-6}, 1.86×10^{-5}, 2.80×10^{-5}) for a series of CH_4 mixing ratios (0.04, 0.10, 0.18, 0.40, 0.99, and 1.96, all % by volume) in 5.0 SLPM of 10% humidified air. For the first six tests [H_2] was kept equal to [CH_4] for each $\alpha_{CH_3O_2}$ determination, and for the last two tests, [H_2] was approximately twice and half the CH_4 mixing ratios of 0.10% and 0.18%, respectively. For each CH_4 mixing ratio, $\alpha_{CH_3O_2}$ is reported as the average of at least four determinations made at each inlet [NO]/[O_2], generated by diluting the air from the calibration assembly by one quarter with O_2 and adding NO to the front injector to generate inlet NO mixing ratios of 3.75, 7.50 and 11.25 ppmV, respectively. The results of this experiment are shown in Fig. 6.

From the first precursor test, the resultant hydroperoxy radical signal from the addition of H_2 did not vary outside the measurement uncertainty with H_2 concentrations

ACPD
10, 22219–22277, 2010

ranging from 0.010% to 0.99%. Thus, the measured $\alpha_{CH_3O_2}$ is significantly less sensitive to the absolute H_2 concentration in the calibration mixture than it is to the concentration of the RO_2 precursor. For this reason, $[H_2]$ was held constant during the second precursor concentration test at a concentration large enough to ensure that the HO_2 radicals measured were formed from the photolysis of water and the reaction of OH with H_2.

The second test involved a series of $\alpha_{CH_3O_2}$ determinations in the two ambient modes, with $[NO]/[O_2]$ ratios of 2.80×10^{-5} and 6.80×10^{-4}. For this test, a wider range of $[CH_4]$ in the air mixture was generated using single and double dilution techniques to add CH_4 to a 5.0 SLPM flow of humidified air. For the single-dilution technique, between 2 and 100 sccm of CH_4 was added directly to the humidified air via a 100 sccm mass flow controller (MFC). The double dilution required an initial step in which a small flow of CH_4 was added to a secondary flow of synthetic air using a 10 sccm MFC and the resulting diluted mixture of CH_4 in air was added to the humidified air via the 100 sccm MFC. During the double dilution, the initial CH_4 in air mixture was vented to maintain a constant pressure approximately 25 mbar above ambient pressure, allowing a constant flow through the 100 sccm MFC. Using the two dilution techniques, calibration-cell methane concentrations ranging from 20 ppmV to 2.0% were generated for subsequent $\alpha_{CH_3O_2}$ measurements. For this experiment, $[H_2]$ in the calibration flow was kept constant at 0.18% for the HO_2 mode of the determinations. The results of this experiment are shown in Fig. 7.

From the second precursor test, it is evident that there are both upper and lower limits for the required concentration of RO_2 precursors in the calibration cell. With decreasing CH_4 concentrations of 0.010% or less, the measured $\alpha_{CH_3O_2,low}$ values for the $HO_2 + RO_2$ mode decrease significantly, most likely due to trace species in the synthetic air reacting with OH in place of CH_4. With increasing calibration-cell methane concentrations of 1.0% or greater, the measured $\alpha_{CH_3O_2}$ values for both measurement modes decrease significantly. In this case, the decrease in $\alpha_{CH_3O_2}$ is likely due to the incomplete chemical conversion of peroxy radicals into H_2SO_4. Thus, for ongoing

ACPD
10, 22219–22277, 2010

calibration purposes, the concentration of RO_2 precursors in the calibration cell should fall between 0.010% and 1.0% equivalent methane reactivity, ideally in the range of 0.05% to 0.2%, corresponding to an OH reactivity of ~60 to 250 s^{-1}.

Using the optimized conditions established for the above calibration cell parameters, i.e. total flow rate through the calibration cell, water vapor concentration in the calibration cell air mixture, and RO_2 precursor concentration, the parameters described in the following sections were explored to better characterize the PeRCIMS instrument.

3.2 PeRCIMS characterization experiments

3.2.1 Ambient pressure dependence

A modified calibration cell that can be sealed onto the sample intake end of the PeRCIMS inlet was used to determine the dependence of $\alpha_{CH_3O_2}$ on ambient pressure. For this test, absolute calibrations and $\alpha_{CH_3O_2}$ determinations were made at the HO_2 and $HO_2 + RO_2$ measurement modes at a range of calibration cell pressures. To achieve a range of pressures at the PeRCIMS intake, a pressure controller and pump were attached to a side port on the calibration cell, downstream of the Hg lamp, to control the pressure in the calibration cell to a desired pressure between 400 and 933 Torr. For these measurements, the air mixture in the cell consisted of 5 SLPM of 10% saturated synthetic air with alternating CH_4 and H_2 at 0.18%, and the flow rates of the reagent gases and diluents were adjusted according to the sample flow rate into the inlet from the calibration cell. The results from this test are listed in Table 4. Fitted slopes of the results for $\alpha_{CH_3O_2}$ versus pressure for the HO_2 and $HO_2 + RO_2$ modes are statistically insignificant at the 98% Confidence Intervals. This is consistent with the inlet being at a constant reduced pressure, and thus the inlet chemistry regulating the conversion of peroxy radicals into H_2SO_4 is independent of the pressure outside the inlet.

The primary concern with regards to ambient pressure is for high-altitude measurements as the sample flow into the inlet can be affected. The flow of gas into the inlet is

ACPD
10, 22219–22277, 2010

proportional to the ambient pressure (P_{amb}) provided $\Delta P/P_{amb} > 0.5$, where ΔP is the difference between ambient P and the inlet P (Green and Perry, 2007). When $\Delta P/P_{amb}$ is less than 0.5, the flow is a function of both the ambient and inlet P. Thus, for ambient pressures less than 300 Torr, the flow through the orifice into a 150 Torr inlet becomes non-linear. Although the inlet chemistry has been optimized for an inlet pressure of 150 Torr, where $P_{amb} < 300$ Torr the inlet pressure can be reduced to 100 Torr to keep the sample flow rate linear with P_{amb}.

3.2.2 RO_2 Precursor characterization

The sensitivity dependence of the PeRCIMS instrument to CH_3O_2 radicals on the ratio of [NO]/[O_2] and on the absolute concentration of [NO] in the inlet have been shown (Fig. 3). However, the general term RO_2 includes many other organic peroxy radical species which may undergo different chemistry in the PeRCIMS inlet. Thus, the sensitivity of the PeRCIMS measurement to organic peroxy radicals other than CH_3O_2 must be quantified.

Edwards et al. (2003) reported a series of α_{RO_2} values for organic peroxy radicals generated via reactions of Cl atoms with a series of RO_2 precursors including alkanes, alkenes and aromatic compounds. These α_{RO_2} were determined at two inlet [NO]: essentially an HO_2 mode and an $HO_2 + RO_2$ mode with inlet [NO]/[O_2] ratios of 1.2×10^{-2} and 2.5×10^{-5}, respectively. In ambient air, however, the majority of RO_2 radicals are formed via OH-oxidation of the parent hydrocarbon. Hence, the α_{RO_2} values that we report here are based on measurements of RO_2 generated from reactions with OH radicals. This is of particular importance for peroxy radicals from OH-reactions with unsaturated non-methane hydrocarbons (NMHC), which typically differ from those generated via unsaturated NMHC-Cl reactions (Orlando et al., 2003; Suh et al., 2003; Taatjes, 1999; Atkinson, 2000). As well, we present measurements of α_{RO_2} for a number of RO_2 precursors at not just two ambient measurement modes, but over a range of inlet [NO] and [O_2].

ACPD
10, 22219–22277, 2010

The same double dilution apparatus discussed in the previous section for adding small flows of methane to the calibration flow was employed here. Gas-phase RO_2 precursors were added via the 10-sccm mass flow controller such that the combined flow rates from the two dilutions resulted in OH reactivities within the optimized range for methane reactivity (60 to 250 s^{-1}). For RO_2 precursors in the liquid phase at room temperature, dry synthetic air was passed through the 10-sccm mass flow controller, then through the headspace of a vial containing a small volume of the precursor. The pressure in the vial and manifold was monitored and vented through a needle valve to maintain a constant pressure approximately 25 mbar above ambient. Thus, the concentration of the precursor in the synthetic air flow could be calculated from its vapor pressure, and an appropriate amount was added to the calibration gas flow to generate OH reactivities in the ideal range.

A total of 17 different NMHC RO_2 precursors were used to create RO_2 radicals that were subsequently measured using the PeRCIMS instrument across a range of [NO]/[O_2]. The results of the α_{RO_2} determinations for each of these precursors were grouped into three different subgroups, C_2–C_5 alkanes (i.e. NMHC with between two and five carbon atoms), C_6–C_7 alkanes, and unsaturated hydrocarbons. These are plotted along with the measurements of $\alpha_{CH_3O_2}$ for comparison in Fig. 8. For some RO_2 precursors, a mixture of RO_2 radicals are generated during reaction with OH and the reported α_{RO_2} values are a weighted mean of the individual values. For each precursor, the mean of all α_{RO_2} determinations made within ±15% of the two ambient measurement modes are shown in Fig. 9, and are also listed in Table 5 with literature OH rate coefficients.

In Fig. 8a, it is clear that the majority of C_2–C_5 NMHC precursors generate RO_2 radicals with similar α_{RO_2} behavior to methylperoxy radicals, but with slightly higher RO_2 sensitivity over the entire [NO]/[O_2] range measured. Overall, the separation between the HO_2-mode and $HO_2 + RO_2$-mode ($\Delta\alpha_{RO_2}$) is similar to methane for each of these RO_2 precursors. The primary exceptions to this are methylpropane with significantly lower α_{RO_2} values over the entire range of [NO]/[O_2] measured, and *n*-pentane

ACPD
10, 22219–22277, 2010

with α_{RO_2} values that deviate from those of the other precursors such that it is much higher than $\alpha_{CH_3O_2}$ in the HO_2 mode region. Possible reasons for these differences are discussed below.

The majority (>70% at or below 298 K) of methylpropane-OH reactions occur via abstraction of the tertiary hydrogen, resulting in a *tert*-butoxy radical after subsequent reaction with NO (Eq. 1) in the PeRCIMS inlet (Atkinson, 1997; Tully et al., 1986). With no α-hydrogen atoms, the *tert*-butoxy radical cannot react with O_2 to generate HO_2 via Reaction (R3). Rather, it either decomposes unimolecularly to generate a methyl fragment which must undergo further reaction in the inlet to generate HO_2 (decomposition lifetime is ~1 ms at 298 K and 760 Torr and is in the fall-off region) (Atkinson, 2007) or react with NO via Reaction (R2) to form *tert*-butylnitrite ($k_{NO,295\ K} = (2.9 \pm 0.2) \times 10^{-11}$ cm^3 s^{-1}, 5 to 80 Torr (Lotz and Zellner, 2000; Atkinson, 2007). With ppmV levels of [NO] in the 150 Torr inlet, *tert*-butoxy + NO is likely much faster than the unimolecular decomposition, hence the sensitivity of the PeRCIMS instrument to *tert*-butylperoxy radicals is low. The signal that is seen from the methylpropane reaction is due to the OH-abstraction of a primary hydrogen atom, resulting in 2-methylpropoxy radicals. The results for 3-methylpentane in Fig. 8b indicate similar behavior, with α_{RO_2} values that tend to be lower than other C_6 alkanes. This is consistent with the formation of alkoxy radicals with no α-hydrogen atoms. However, this behavior is not evident in the methylbutane and 2-methylpentane results (Fig. 8a and b), both having α_{RO_2} values closer to the *n*-alkane with the same number of straight-chain carbon atoms.

From the *n*-pentane precursor reactions, the measured α_{RO_2} values are increasingly larger than $\alpha_{CH_3O_2}$ values with increasing [NO]/[O_2], as are the α_{RO_2} values from the C_6 and C_7 alkane precursors in Fig. 8b. This is most likely due to *n*-pentane and larger alkanes having sufficient numbers of carbon atoms to generate alkoxy radicals that are subject to isomerization. These isomerizations often result in reactions that generate HO_2 radicals, lowering the separation dependence on the [NO]/[O_2] ratio. Figure 8a and b show that as the numbers of carbon atoms in alkanes increase, the

ACPD
10, 22219–22277, 2010

ability to deselect the resultant RO_2 radical in the HO_2 mode decreases, and thus the separation between HO_2 and $HO_2 + RO_2$ becomes smaller.

In Fig. 8c, the α_{RO_2} values from the unsaturated NMHC precursors have a similar dependence on [NO]/[O_2] as larger alkane RO_2 precursors. In general, alkene-OH reactions occur as addition reactions, forming hydroxyalkyl radicals that react with O_2 under atmospheric conditions to form β-hydroxyalkyl peroxy radicals (and δ-hydroxyalkyl peroxy radicals where conjugated double bonds are present). In high [NO] environments (i.e. the PeRCIMS inlet), these peroxy radicals react with NO forming primarily hydroxyalkoxy radicals that can decompose unimolecularly (typically generating HO_2), isomerize or react with O_2 to carbonyl compounds and HO_2 (Atkinson, 1997). Thus, in the PeRCIMS inlet, (R2) is unsuitable for suppression of the conversion of the hydroxyalkoxy radical to HO_2 for alkene-precursor RO_2 and therefore the separation between HO_2 and $HO_2 + RO_2$ is lessened. Aromatic hydrocarbons undergo a combination of addition and abstraction reactions with OH radicals (Atkinson, 2000), so with benzene and toluene as RO_2 precursors, the impact of rearrangement and dissociation leading to HO_2 is seen in the measured α_{RO_2}, but to a lesser degree. Overall, due to the differences in sensitivity of the PeRCIMS to different RO_2 radicals, reported measurements of ambient $HO_2 + RO_2$ and HO_2 must account for the relative reactivity of RO_2 precursors in the air masses being studied.

3.2.3 Standard model vs. analytical model

Applying standard tropospheric chemistry to the inlet yields the expected behavior of equal yields of H_2SO_4 from HO_2 and CH_3O_2 radicals at small [NO]/[O_2] ($\alpha = 1$), and small yields of H_2SO_4 for RO_2 relative to HO_2 at large [NO]/[O_2] ($\alpha \rightarrow 0$). This standard model was presented in Edwards et al. (2003), and is shown in Fig. 3a. It can be seen that the observations of $\alpha_{CH_3O_2}$ differ significantly from the standard model for low [NO]/[O_2] and, unexpectedly, values greater than unity were measured. This implies that processes dependent on both the inlet [NO]/[O_2] ratio (Fig. 3a) and the absolute [NO] in the inlet (Fig. 3b) are operative which produce more than one HO_2 per RO_2

ACPD
10, 22219–22277, 2010

for these conditions, or that H_2SO_4 is produced in addition to the conversion to HO_2. On the other hand, agreement between the observations and the standard model at large [NO]/[O_2] values is reasonable, in contrast to the results of Edwards et al. (2003) (Fig. 3a). We believe that the larger than expected α values observed by Edwards et al. were due to contaminants in the zero air used in their experiments. We found it necessary to use the cleanest synthetic air available (so-called Hydrocarbon Free, with VOC content less than 0.1 ppmV) to avoid this artifact. Edwards and colleagues did not observe the larger than unity α values at low [NO]/[O_2], likely because their measurements were not made at sufficiently low [NO]/[O_2] ratios (minimum ratio of 2.8×10^{-5}).

What reactants could convert SO_2 into H_2SO_4 and/or RO_2 into HO_2 with yields leading to apparent α values greater than unity at low [NO]/[O_2], while maintaining the inefficient conversion at high [NO]/[O_2]? Possible candidates are RO_2 and RO, or unknown chemistry involving OH and/or HO_2. RO would seem reasonable by analogy with OH. RO_2 is unlikely, although several papers appear in the literature discuss the oxidation of SO_2 by CH_3O_2 (e.g., Kan et al., 1981 and references therein). Current thinking is that the direct oxidation of SO_2 is quite slow ($<10^{-16}$ cm^3 molecule^{-1} s^{-1} Sander and Watson, 1981). On the other hand, Kan et al. (1981) argue for a multiple-step mechanism involving two equilibria, which results in the oxidation of SO_2 while preserving the CH_3O_2 radicals.

Yields of HO_2 and H_2SO_4 from the reactions of RO_2 radicals within the instrument inlet were calculated in the following way, and compared with the laboratory measured values. Each RO_2 precursor reacts with OH to produce one or more isomers. The yields of these isomers have been reported in the literature for some reactants, and structure activity relationships have been developed to predict the isomer yields (Calvert et al., 2008; Kwok and Atkinson, 1995; Neeb, 2000). We used the method of Calvert et al. for the alkane precursors, and that of Neeb for the others. Several reactions between the radicals and the reagent gases within the inlet are part of standard

ACPD
10, 22219–22277, 2010

tropospheric chemistry.

$$RO_2 + NO \rightarrow RO + NO_2 (+M) \rightarrow RONO_2 \quad \text{(R17)}$$

$$RO + O_2 \rightarrow R'R''CO + HO_2 \quad \text{(R18)}$$

$$RO + M \rightarrow R'^{\cdot} + R''CHO \quad \text{(R19)}$$

$$RO \rightarrow HO{-}R'^{\cdot} + O_2 + M \rightarrow HO{-}RO_2 + M. \quad \text{(R20)}$$

Following isomerization (R20) or decomposition (R19), the alkyl radical adds to O_2 to form a new organic peroxy radical, which cascades through the sequence. When produced, HO_2 reacts as described earlier. We found it not possible to explain our laboratory observations of the sensitivity of RO_2 radicals in our instrument. Missing from this chemistry are reactions between peroxy and alkoxy radicals and SO_2. Although not recognized as relevant to tropospheric chemistry, based on analogy with OH and HO_2, we might speculate that RO would react with SO_2 leading to SO_3 and other products. Edwards et al. (2003) proposed a reaction between CH_3O and SO_2 to explain their observation of higher than expected H_2SO_4 yields at high [NO]/[O_2] ratios. No detailed mechanism was proposed, other than to indicate that H_2SO_4 was eventually produced along with other non-radical or slowly reacting products.

Kan et al. (1981) reported results of detailed laboratory chamber studies of the kinetics and mechanism of reactions between CH_3O_2, CH_3O and CH_3 with SO_2 in the presence of O_2 and NO. They argue that these reactions involve multiple equilibria between the radicals, SO_2 and O_2. They also explain that conventional flow tube kinetics studies do not observe a reaction between CH_3O_2 and SO_2 due to the absence of O_2, resulting in the recommended (Sander et al., 2006) rate coefficient for $CH_3O_2 + SO_2$ at an upper limit of 5×10^{-17} cm^3 molecule^{-1} s^{-1}. This is discussed in a footnote in Sander et al. (2006) with the conclusion that the decomposition of the $CH_3O_2SO_2$ adduct back to CH_3O_2 and SO_2 likely dominates under atmospheric conditions. While this may be true, we seek a mechanism for the production of additional HO_2 and/or

ACPD
10, 22219–22277, 2010

H_2SO_4 in our instrument inlet. We hypothesize that there are three potential mechanisms that produce H_2SO_4 without consumption of radicals. Mechanism (a) involves the reaction between RO_2 and SO_2 along the lines of Kan et al. (1981)

$$RO_2 + SO_2 + M \rightarrow RO_2SO_2 + M \quad \text{(R21)}$$

$$RO_2SO_2 + O_2 + M \rightarrow RO_2SO_2O_2 + M \quad \text{(R22)}$$

The $RO_2SO_2O_2$ behaves like any other peroxy radical, primarily reacting with NO in our inlet.

$$RO_2SO_2O_2 + NO \rightarrow RO_2SO_2O + NO_2 \quad \text{(R23)}$$

The alkoxy radical produced could potentially undergo a number of reactions, but decomposition is most likely.

$$RO_2SO_2O \rightarrow RO_2 + SO_3 \quad \text{(R24)}$$

This mechanism produces SO_3 and eventually H_2SO_4 without consumption of radicals, and has the potential to explain our laboratory measurements. Overall, the reaction involves the catalytic oxidation of SO_2 to SO_3.

$$RO_2 + SO_2 + O_2 + NO \rightarrow\rightarrow RO_2 + SO_3 + NO_2 \quad \text{(R25)}$$

Mechanism (b), also discussed by Kan et al. (1981), involves the reaction between RO and SO_2 resulting in production of RO and SO_3. The chemistry is similar to that shown for $RO_2 + SO_2$, with the final reaction involving the decomposition of $ROSO_2O$ into RO and SO_3 and an overall reaction:

$$RO + SO_2 + O_2 + NO \rightarrow\rightarrow RO + SO_3 + NO_2 \quad \text{(R26)}$$

Mechanism (c) involves reaction between RO and SO_2 leading to RO_2 and SO_3. This is only slightly different than mechanism (b), but will lead to lower yields when the nitrate yield in the reaction of RO_2 with NO is significant.

$$RO + SO_2 + M \rightleftharpoons ROSO_2 + M \quad \text{(R27)}$$

ACPD
10, 22219–22277, 2010

$$ROSO_2 + O_2 \rightarrow RO_2 + SO_3 \quad \text{(R28)}$$

$$ROSO_2 + M \rightarrow R + SO_3 \quad \text{(R29)}$$

$$R + O_2 + M \rightarrow RO_2 + M \quad \text{(R30)}$$

Overall, this mechanism converts RO and SO_2 into RO_2 and SO_3.

$$RO + SO_2 + O_2 \rightarrow\rightarrow RO_2 + SO_3 \quad \text{(R31)}$$

The rate laws for each of these mechanisms is similar, if we assume that the reaction of the sulfur-containing peroxy radical with NO is not rate limiting. In that case, the production rate of SO_3 is given by the following.

$$\left(\frac{d[SO_3]}{dt}\right)_a = k_a[O_2][SO_2][RO_2] \quad (5)$$

Similar equations apply to mechanisms (b) and (c). Equations for the production of HO_2 from Reactions (R1–R7), and mechanisms (a–c) were derived and used to predict the yield of H_2SO_4 from RO_2 relative to HO_2 for each of the isomers produced in the reactions of OH with the various precursors studied. The rate coefficients, k_a, k_b, and k_c were used as fit parameters. In addition, the rate coefficients for RO + NO reactions for alkanes larger than C_3 and the other species were allowed to vary within a range (5×10^{-12} to 4×10^{-11} cm^3 $molecule^{-1}$ s^{-1}) as part of the fitting procedure. The rate coefficients for $RO + O_2$ were set to their recommended values (1×10^{-14} for primary RO and 8×10^{-15} for secondary RO), and to zero for tertiary RO. In a few cases, no satisfactory fit could be found varying the four rate coefficients, and in those cases the rate coefficients for $RO + O_2$ were also fit. RO_2 + NO rate coefficients were set to recommended values for smaller RO_2 (C_3 and smaller alkanes), and to 8×10^{-12} for larger alkanes and the other species. Using this approach, the laboratory observations were reproduced with remarkable accuracy.

ACPD
10, 22219–22277, 2010

The rate coefficients yielding the best fits for the RO + NO reactions were in the $3 - 4 \times 10^{-11}$ range for C_6 and smaller alkanes. The C_7 alkane was 1×10^{-11}, while for the alkenes the best fit was 5×10^{-12}. For the aromatics, the values needed to be set at the kinetic limit of about 4×10^{-10}. The rate coefficient for mechanism (a) averaged approximately 1×10^{-31} cm^6 molecule^{-2} s^{-1}, resulting in a value of $k_a[O_2]$ at low [NO]/[O_2] ratios of about 3×10^{-13} cm^3 molecule^{-1} s^{-1}, and about 5×10^{-14} at high [NO]/[O_2] ratios. These values are larger than the value recommended by Kan et al. (1981) of 1.4×10^{-14} cm^3 molecule^{-1} s^{-1}. There is variability in the best values for k_a. For example, it is about 1×10^{-36} cm^6 molecule^{-2} s^{-1} for *tert*-butoxy radicals. Values are also similar for 2- and 3-heptylperoxy radicals. Some best fit values are zero (e.g. for 2- and 3-hexylperoxy, and many of the tertiary peroxy radicals) while the value for 1-hexylperoxy is unrealistically large (2×10^{-26} cm^6 molecule^{-2} s^{-1}). This is likely an artifact of the fitting procedure. Rate coefficients for mechanism (b) range from 10^{-31} to 10^{-27} with the straight-chained peroxy radicals tending to have the higher values. Tertiary peroxy radicals often have zero values. The radicals derived from alkenes are generally at the low end, mostly between 2×10^{-31} and 10^{-29}. Finally, the rate coefficients for mechanism (c) range from 10^{-32} to 10^{-29}. Values are zero for isoprene and the aromatics, and mid-10^{-32} for the other alkenes. Overall, for most peroxy radicals, mechanism (a) accounts for most of the effect of increasing the yield of H_2SO_4 from RO_2 in our inlet. Mechanism (b) seems to more important for alkenes (along with (a)), and (c) only has an impact for a few specific isomers (e.g. 2- and 3-hexylperoxy and 4-heptylperoxy). The revised inlet chemistry for RO_2 and HO_2 in the PeRCIMS inlet based on this fit is shown in Schemes 1 and 2. We clearly need more kinetic data to constrain these mechanisms, but it appears that the reactions between RO_2 and RO with SO_2 in the presence of O_2 and NO are operative in our inlet and contribute significantly to the signals we observe. It is our intent to study this chemistry further and in a future paper to examine its impacts in the atmosphere.

ACPD
10, 22219–22277, 2010

4 Ambient measurements

For ambient peroxy radical measurements, a fraction of the peroxy radicals measured in the HO_2 mode are RO_2 radicals. The actual HO_2 concentration $[HO_2]_{amb}$ in an individual HO_2-mode measurement can be approximated using the previous and subsequent measurements in the $HO_2 + RO_2$ mode. Likewise, the actual concentration of $HO_2 + RO_2$ in an individual $HO_2 + RO_2$-mode measurement can be approximated using previous and subsequent measurements in the HO_2 mode. Ambient HO_2 and RO_2 concentrations are thus determined using the following:

$$[HO_2]_{amb} = S_{low}F_{low} - \alpha_{low}\left[\frac{S_{low}F_{low} - S_{high}F_{high}}{\alpha_{low} - \alpha_{high}}\right] \quad (6)$$

$$[RO_2]_{amb} = \frac{S_{low}F_{low} - S_{high}F_{high}}{\alpha_{low} - \alpha_{high}} \quad (7)$$

The term S_{low} is equal to $S_{HO_2,low} + S_{RO_2,low}$, the sum of the signals due to HO_2 and RO_2 in the $HO_2 + RO_2$ mode or low $[NO]/[O_2]$ mode. Likewise S_{high} is equal to $S_{HO_2,high} + S_{RO_2,high}$, the sum of the signals due to HO_2 and RO_2 in the HO_2 mode or high $[NO]/[O_2]$ mode. The terms F_{low} and F_{high} are the calibration factors for the $HO_2 + RO_2$ and HO_2 modes, respectively, and are defined as:

$$F_{low} = [HO_2]_{H_2}/S_{H_2,low} \quad (8)$$

$$F_{high} = [HO_2]_{H_2}/S_{H_2,high} \quad (9)$$

From Eq. (2), the absolute concentration of HO_2, $[HO_2]_{H_2}$, in both modes is $2(It)\sigma_{H_2O}\phi_{H_2O}[H_2O]$. Finally, α_{high} and α_{low} are the measurement sensitivities to RO_2 (relative to HO_2) at the two ambient measurement modes with high $[NO]/[O_2]$ and low $[NO]/[O_2]$ and are defined as:

$$\alpha_{high} = \frac{S_{RO_2,high}}{S_{HO_2,high}} \quad (10)$$

ACPD
10, 22219–22277, 2010

$$\alpha_{low} = \frac{S_{RO_2,low}}{S_{HO_2,low}} \quad (11)$$

The values of F_{low}, F_{high}, α_{high} and α_{low} are determined during laboratory instrument characterizations and absolute calibration measurements.

Because the ambient concentration of RO_2 is not measured independently from HO_2, it is subject to greater uncertainty as it relies on the difference of two measured signals. Thus, we recommend that ambient data are reported as HO_2 and $HO_2 + RO_2$ concentrations, such that reported $HO_2 + RO_2$ concentrations are the combination of both $[HO_2]$ and $[RO_2]$, and are essentially the HO_2 + RO_2-mode signal with a small correction:

$$[HO_2 + RO_2]_{amb} = S_{low}F_{low} + \frac{(1-\alpha_{low})(S_{low}F_{low} - S_{high}F_{high})}{\alpha_{low} - \alpha_{high}} \quad (12)$$

which can be simplified to:

$$[HO_2 + RO_2]_{amb} = \frac{S_{low}F_{low}(1-\alpha_{high}) - S_{high}F_{high}(1-\alpha_{low})}{\alpha_{low} - \alpha_{high}} \quad (13)$$

Thus, both $[HO_2]_{amb}$ and $[HO_2 + RO_2]_{amb}$ are determined using the signals measured during both the HO_2 and the HO_2 + RO_2 modes, and the α values for each mode. For this reason, for each HO_2 mode measurement, $[HO_2]_{amb}$ is calculated using the average of the previous and following signal measurements in the $HO_2 + RO_2$ mode, $S_{low,ave}$, and likewise, $[HO_2 + RO_2]_{amb}$ is calculated using the average of the previous and following signal measurements in the HO_2 mode, $S_{high,ave}$.

4.1 Ambient data from the MIRAGE and INTEX-B campaigns

In Spring 2006, the PeRCIMS instrument was deployed on the NSF/NCAR C-130 during the MIRAGE-Mex and INTEX-B field campaigns, described in detail in an overview paper (Singh et al., 2009). The MIRAGE-Mex (Megacities Impact on Regional and

ACPD
10, 22219–22277, 2010

Global Environment-Mexico City) campaign, which took place in March 2006, was designed to investigate the chemical and physical transformation of gases and aerosol in the polluted outflow from Mexico City. INTEX-B, the second phase of NASA's Intercontinental Transport Experiment which took place during April-May 2006, was designed to quantify the transpacific transport and evolution of Asian pollution to North America. Concentrations of NO were also measured on the C-130 by chemiluminescence (Ridley et al., 2004). Following the field studies, the NASA Langley time-dependent photochemical box model (Crawford et al., 1999; Olson et al., 2001, 2006; Fried et al., 2008a, b) was used to estimate radical concentrations along the flight tracks of a number of the C-130 flights, constrained by observations of other chemical species made onboard the aircraft.

Time-series plots of segments of the C-130 flights on 10 March 2006 and 3 May 2006 are shown in Fig. 10a and b. Both plots include observations and modeled HO_2 and $HO_2 + RO_2$ mixing ratios as well as GPS altitude, 1-Hz [NO] observations and 1-min averaged [NO]. In these plots, which are fairly typical for the two field campaigns, the observations and model output are generally in good agreement, but under certain conditions the measured and modeled peroxy radical concentrations deviate significantly. For example, when [NO] > 0.5 ppbV, (both 1-Hz and 1-min averaged [NO]) the model-predicted $HO_2 + RO_2$ mixing ratios are much lower than the actual observed radical concentrations, and to a lesser extent, the model-predicted HO_2 mixing ratios are lower than the observed data. This tendency for the measurement/model ratio to increase with increasing NO_x has been discussed previously for measurements of hydroperoxy radicals and hydroxyl radicals (Faloona et al., 2000; Ren et al., 2005, 2006; Olson et al., 2006). The discrepancy between measurements and model with high NO_x for the peroxy radical data from MIRAGE-Mex, INTEX-B and other more recent campaigns will be explored further in a separate paper. Other times the observations and model differed significantly during the 2006 campaigns occurred when the C-130 was in air masses heavily influenced by biomass burning, and in the marine boundary layer.

ACPD
10, 22219–22277, 2010

Overall, there were six C-130 MIRAGE-Mex flights and eight INTEX-B flights with both observations and box model peroxy radical data available for comparison. In total, there were approximately 2700 HO_2 and 3000 $HO_2 + RO_2$ data points with both ambient and model values. Excluding data points with measured or modeled peroxy mixing ratios <2 pptV as well as those with corresponding 1-min average [NO] > 0.5 ppbV, there are approximately 2500 HO_2 and 2800 $HO_2 + RO_2$ data points remaining for comparison. From these, the mean measurement/model ratios for the MIRAGE-Mex flights were 1.25 ± 0.74 (HO_2) and 1.54 ± 0.73 ($HO_2 + RO_2$), and for the INTEX flights, 1.15 ± 0.58 (HO_2) and 1.36 ± 0.77 ($HO_2 + RO_2$).

Both of these data sets will be thoroughly explored in separate papers. In general, however, the observations tend to be larger than the box model predicts, with more deviation between measurement and model during the MIRAGE-Mex campaign. The observations of [HO_2] and [$HO_2 + RO_2$] during these campaigns demonstrate that we are able to measure separated hydroperoxy and organic peroxy radical concentrations on timescales relevant for fast photochemistry and useful for comparison to O-D photochemical models of aircraft observations.

4.2 Impact of alpha value uncertainties

The reported α_{high,CH_3O_2} and α_{low,CH_3O_2} values for the HO_2 and $HO_2 + RO_2$ measurement modes are 0.17 ± 0.04 and 1.22 ± 0.08. To determine the impact of the reported uncertainties, we used the data set from the 10 March MIRAGE-Mex flight. By changing the α_{high} value by ±25% (the estimated uncertainty), the individual calculated [HO_2] changed by less than 3% on average. The calculated [$HO_2 + RO_2$] changed by less than 1%. Similarly, by changing α_{low} the value by ±7%, the calculated [HO_2] and [$HO_2 + RO_2$] change by less than 1% and 2%, on average, respectively. These changes are all well within the reported peroxy radical measurement uncertainties of ~30%.

However, what the reported $\alpha_{CH_3O_2}$ uncertainties do not directly account for is the impact on α_{high} and α_{low} due to organic peroxy radicals other than CH_3O_2. As shown

ACPD
10, 22219–22277, 2010

in Fig. 8a–c, the [NO]/[O_2] dependence of α_{RO_2} values for some RO_2 precursors can vary significantly from that of methane. For this reason, it is important to consider the impact that RO_2 precursor speciation can have on the uncertainty of both calculated HO_2 and $HO_2 + RO_2$ concentrations.

To estimate the impact of non-CH_3O_2 RO_2 on the uncertainties of the reported [HO_2] and [$HO_2 + RO_2$] in the MIRAGE-Mex and INTEX-B data sets, we assessed the RO_2 precursor loading for different types of air masses measured during a MIRAGE-Mex flight, and looked at the measurement/model ratios with respect to the box modeled fraction of total RO_2 that is CH_3O_2 for both campaigns full data sets.

During the 10 March flight, the C-130 sampled air masses with a variety of RO_2 precursors at a wide range of relative concentrations. The NASA LaRC box model output for the non-CH_3O_2 RO_2 along the flight track is the sum of 25 parameterized RO_2 groups based on precursor type and oxidant. The chemical scheme for non-methane hydrocarbons in the box model derives from that in the lumped scheme of Lurmann et al. (1986), with updates as described in Crawford et al. (1999) and Olson et al. (2006). The 25 functional peroxy groups are described in Table 6. A plot of the fraction of the total RO_2 comprised of these 25 RO_2 groups and CH_3O_2 according to the model for this flight is shown in Fig. 11. During the flight, the CH_3O_2 fraction is predicted to range from 16% to 92% of the total RO_2. Based on the experiments with NMHC RO_2 precursors, the PeRCIMS inlet is not sensitive to all RO_2 species equally. As well, there are a number of RO_2 radicals that are converted into HO_2 in the HO_2 mode, and are thus included in the observed [HO_2]. The 25 RO_2 groups in Fig. 11 have been colored according to the sensitivity of the PeRCIMS measurement: blue-toned groups are those that are primarily observed in the RO_2 mode, red-toned groups are those that primarily generate a signal in the HO_2 mode, and the green-toned groups contain a mixture of RO_2 radicals that may be observed as RO_2 or HO_2.

From Fig. 11, at some points during the flight, as much as 50% of the ambient RO_2 could be measured in the HO_2 mode. This implies that the observed [HO_2] would be greater than the modeled [HO_2] in regions where the CH_3O_2 RO_2 fraction is low. In

ACPD
10, 22219–22277, 2010

Fig. 12, a plot of the observed [HO_2] and [$HO_2 + RO_2$] and modeled [HO_2], [CH_3O_2] and non-CH_3O_2 [RO_2] for the 10 March flight, it is not clear that there is less observed [RO_2] or an excess of observed [HO_2] in comparison to the model at any point during the flight. Indeed, the observations and the model either agree quite well or the observed [HO_2] and [$HO_2 + RO_2$] exceed that of the model. This suggests there are RO_2 and/or RO_2 precursors that are not being accounted for in the model or by the VOC measurements, either in the gas or the aerosol phase.

It is possible that much of the observed RO_2 that is not accounted for by the box model is a product of the OH-oxidation of acetaldehyde, CH_3CO_3. According to Apel et al. (2010), the two VOCs with the greatest influence on OH reactivity in the Mexico City Metropolitan Area (MCMA) region are acetaldehyde and formaldehyde. The NASA LaRC box model is not constrained by acetaldehyde observations, and the model-predicted acetaldehyde concentrations are on average half the observed [acetaldehyde] measured onboard the C-130 by the NCAR Trace Organic Gas Analyzer (TOGA) instrument while it was in the region of the MCMA during the 10 March flight (Fig. 12, top panel). During this time, approximately 20:30–23:20 UTC, the observed [$HO_2 + RO_2$] was higher than the modeled [$HO_2 + RO_2$]. The PeRCIMS is sensitive to CH_3CO_3 as RO_2 (MCO3 in Table 6), so it is likely that lower predicted acetaldehyde concentrations contribute to the modeled [$HO_2 + RO_2$] being lower than the observed [$HO_2 + RO_2$]. However, this is likely only a part of the overall RO_2 signal missing from the model, as doubling the MCO3 contribution in Fig. 11 would not account for a significant increase in modeled RO_2.

5 Conclusions

An improved method for separating and measuring hydroperoxy and organic peroxy radicals has been developed and characterized extensively for both ground-based and airborne measurements. The method builds upon previously described CIMS techniques for measuring peroxy radicals in that both HO_2 and HO_2+RO_2 modes can be observed each minute, with improved separation between modes.

ACPD
10, 22219–22277, 2010

Operationally, the use of NO and SO_2 mixtures that can be used in both measurement modes by simply increasing or decreasing the flow rates by a factor of 4.5 has allowed for significantly faster switching between measurement modes than previously possible with pure reagent gases. By diluting the sample 1:1 with diluent gases, the overall measurement sensitivity has been effectively halved. However, compared to the fourfold dilution used by Hanke et al. (2002), this method allows for a higher degree of sensitivity by only diluting the sample flow by half and combining the dilution with two inlet NO mixing ratios. Most importantly, because α_{RO_2} in the HO_2 mode is only ~0.2 for CH_3O_2, $CH_3CH_2O_2$ and other simple organic peroxy radicals, we are able to successfully separate HO_2 and RO_2 for the majority of atmospheric conditions over a wide range of RO_2 precursor concentrations and mixtures. Undermeasurement of [RO_2] and overmeasurement of [HO_2] due to conversion in the inlet in the HO_2 mode may occur in regions where unsaturated hydrocarbons are present in high concentrations. However, the observed [RO_2] during a MIRAGE-Mex flight are on average higher than the model predicts in these circumstances, indicating that there are likely additional sources of RO_2 that are not being accounted for in the model.

6 Acknowledgements

The authors thank Fred Eisele and Edward Kosciuch for their instrument expertise and advice, Andrew Wienheimer for providing the NO_x data from the MIRAGE and INTEX field campaigns, and the crew and support team for the NSF/NCAR C-130 aircraft. The authors also thank Geoff Tyndall and Wengang Zheng for helpful discussion. The authors gratefully acknowledge the financial support of NASA NNG06GB67G. The National Center for Atmospheric Research is operated by the University Corporation for Atmospheric Research under the sponsorship of the National Science Foundation.

ACPD
10, 22219–22277, 2010

References

Apel, E. C., Emmons, L. K., Karl, T., Flocke, F., Hills, A. J., Madronich, S., Lee-Taylor, J., Fried, A., Weibring, P., Walega, J., Richter, D., Tie, X., Mauldin, L., Campos, T., Weinheimer, A., Knapp, D., Sive, B., Kleinman, L., Springston, S., Zaveri, R., Ortega, J., Voss, P., Blake, D., Baker, A., Warneke, C., Welsh-Bon, D., de Gouw, J., Zheng, J., Zhang, R., Rudolph, J., Junkermann, W., and Riemer, D. D.: Chemical evolution of volatile organic compounds in the outflow of the Mexico City Metropolitan area, Atmos. Chem. Phys., 10, 2353–2375, doi:10.5194/acp-10-2353-2010, 2010.

Atkinson, R.: Gas-phase tropospheric chemistry of volatile organic compounds. 1. Alkanes and alkenes, J. Phys. Chem. Ref. Data, 26, 215–290, 1997.

Atkinson, R.: Atmospheric chemistry of VOCs and NO_x, Atmos. Environ., 34, 2063–2101, 2000.

Atkinson, R. and Arey, J.: Atmospheric degredation of volatile organic compounds, Chem. Rev., 103, 4605–4638, doi:10.1021/cr0206420, 2003.

Atkinson, R.: Rate constants for the atmospheric reactions of alkoxy radicals: an updated estimation method, Atmos. Environ., 41, 8468–8485, doi:10.1016/j.atmosenv.2007.07.002, 2007.

Calvert, J. G., Derwent, R. G., Orlando, J. J., Tyndall, G. S., and Wallington, T. J.: Mechanisms of the Atmospheric Oxidation of the Alkanes, Oxford University Press, New York, 2008.

Cantrell, C. A., Zimmer, A., and Tyndall, G. S.: Absorption cross sections for water vapor from 183 to 193 nm, Geophys. Res. Lett., 24, 2195–2198, 1997a.

Cantrell, C. A., Zimmer, A., and Tyndall, G. S.: Absorption cross sections for water vapor from 183 to 193 nm (vol. 24, pg. 2195, 1997), Geophys. Res. Lett., 24, 2687–2687, 1997b.

Cantrell, C. A., Mauldin, L., Zondlo, M., Eisele, F., Kosciuch, E., Shetter, R., Lefer, B., Hall, S., Campos, T., Ridley, B., Walega, J., Fried, A., Wert, B., Flocke, F., Weinheimer, A., Hannigan, J., Coffey, M., Atlas, E., Stephens, S., Heikes, B., Snow, J., Blake, D., Blake, N., Katzenstein, A., Lopez, J., Browell, E. V., Dibb, J., Scheuer, E., Seid, G., and Talbot, R.: Steady state free radical budgets and ozone photochemistry during TOPSE, J. Geophys. Res., 108, 8361, 2003a.

Cantrell, C. A., Edwards, G. D., Stephens, S., Mauldin, L., Kosciuch, E., Zondlo, M., and Eisele, F.: Peroxy radical observations using chemical ionization mass spectrometry during TOPSE, J. Geophys. Res., 108, 8371, 2003b.

ACPD
10, 22219–22277, 2010

Cantrell, C. A., Edwards, G. D., Stephens, S., Mauldin, R. L., Zondlo, M. A., Kosciuch, E., Eisele, F. L., Shetter, R. E., Lefer, B. L., Hall, S., Flocke, F., Weinheimer, A., Fried, A., Apel, E., Kondo, Y., Blake, D. R., Blake, N. J., Simpson, I. J., Bandy, A. R., Thornton, D. C., Heikes, B. G., Singh, H. B., Brune, W. H., Harder, H., Martinez, M., Jacob, D. J., Avery, M. A., Barrick, J. D., Sachse, G. W., Olson, J. R., Crawford, J. H., and Clarke, A. D.: Peroxy radical behavior during the Transport and Chemical Evolution over the Pacific (TRACE-P) campaign as measured aboard the NASA P-3B aircraft, J. Geophys. Res., 108, 8797, doi:10.1029/2003JD003674, 2003c.

Crawford, J., Davis, D., Olson, J., Chen, G., Liu, S., Gregory, G., Barrick, J., Sachse, G., Sandholm, S., Heikes, B., Singh, H., and Blake, D.: Assessment of upper tropospheric HO_x sources over the tropical Pacific based on NASA GTE/PEM data: Net effect on HO_x and other photochemical parameters, J. Geophys. Res., 104, 16255–16273, 1999.

Edwards, G. D., Cantrell, C. A., Stephens, S., Hill, B., Goyea, O., Shetter, R. E., Mauldin, R. L., Kosciuch, E., Tanner, D. J., and Eisele, F. L.: Chemical ionization mass spectrometer instrument for the measurement of tropospheric HO_2 and RO_2, Anal. Chem., 75, 5317–5327, 2003.

Faloona, I., Tan, D., Brune, W. H., Jaegle, L., Jacob, D. J., Kondo, Y., Koike, M., Chatfield, R., Pueschel, R., Ferry, G., Sachse, G., Vay, S., Anderson, B., Hannon, J., and Fuelberg, H.: Observations of HO_x and its relationship with NO_x in the upper troposphere during SONEX, J. Geophys. Res., 105, 3771–3783, 2000.

Fried, A., Walega, J. G., Olson, J. R., Crawford, J. H., Chen, G., Weibring, P., Richter, D., Roller, C., Tittel, F. K., Heikes, B. G., Snow, J. A., Shen, H., O'Sullivan, D. W., Porter, M., Fuelberg, H., Halland, J., and Millet, D. B.: Formaldehyde over North America and the North Atlantic during the summer 2004 INTEX campaign: methods, observed distributions, and measurement-model comparisons, J. Geophys. Res., 113, D10302, doi:10.1029/2007JD009760, 2008a.

Fried, A., Olson, J. R., Walega, J. G., Crawford, J. H., Chen, G., Weibring, P., Richter, D., Roller, C., Tittel, F., Porter, M., Fuelberg, H., Halland, J., Bertram, T. H., Cohen, R. C., Pickering, K., Heikes, B. G., Snow, J. A., Shen, H., O'Sullivan, D. W., Brune, W. H., Ren, X., Blake, D. R., Blake, N., Sachse, G., Diskin, G. S., Podolske, J., Vay, S. A., Shetter, R. E., Hall, S. R., Anderson, B. E., Thornhill, L., Clarke, A. D., McNaughton, C. S., Singh, H. B., Avery, M. A., Huey, G., Kim, S., and Millet, D. B.: Role of convection in redistributing formaldehyde to the upper troposphere over North America and the North Atlantic during the sum-

ACPD
10, 22219–22277, 2010

mer 2004 INTEX campaign, J. Geophys. Res., 113, D17306, doi:10.1029/2007JD009760, 2008b.
Fuchs, H., Holland, F., and Hofzumahaus, A.: Measurement of tropospheric RO_2 and HO_2 radicals by a laser-induced fluorescence instrument, Rev. Sci. Instrum., 79, 084104, doi:10.1063/1.29687121, 2008.
Green, D. W. and Perry, R. H.: Perry's Chemical Engineers' Handbook, 8th Edition, McGraw-Hill, United States, 2007.
Green, T. J., Reeves, C. E., Fleming, Z. L., Brough, N., Richard, A. R., Bandy, B. J., Monks, P. S., and Penkett, S. A.: An improved dual channel PERCA instrument for atmospheric measurements of peroxy radicals, J. Environ. Monitor., 8, 530–536, doi:10.1039/b514630e, 2006.
Hanke, M., Uecker, J., Reiner, T., and Arnold, F.: Atmospheric peroxy radicals: ROXMAS, a new mass-spectrometric methodology for speciated measurements of HO_2 and ΣRO_2 and first results, Int. J. Mass Spectrom., 213, 91–99, 2002.
Hasson, A. S., Chung, M. Y., Kuwata, K. T., Converse, A. D., Krohn, D., and Paulson, S. E.: Reaction of Criegee intermediates with water vapor – An additional source of OH radicals in alkene ozonolysis?, J. Phys. Chem. A, 107, 32, 6176–6182, doi:10.1021/jp0346007, 2003.
Kan, C. S., Calvert, J. G., and Shaw, J. H.: Oxidation of Sulfur-Dioxide by Methylperoxy Radicals, J. Phys. Chem., 85, 1126–1132, 1981.
Kwok, E. S. C. and Atkinson, R.: Estimation of hydroxyl radical reaction rate constants for gas-phase organic compounds using a structure-reactivity relationship: an update, Atmos. Environ., 29, 1685–1695, 1995.
Lotz, C. and Zellner, R.: Fluorescence excitation spectrum of the *tert*-butoxy radical and kinetics of its reactions with NO and NO_2, Phys. Chem. Chem. Phys., 2, 2353–2360, 2000.
Lurmann, F. W., Lloyd, A. C., and Atkinson, R.: A chemical mechanism for use in long-range transport/acid deposition computer modeling, J. Geophy. Res., 91, D10, 10905–10936, 1986.
Neeb, P.: Structure-reactivity based estimation of the rate constants for hydroxyl radical reactions with hydrocarbons, J. Atmos. Chem., 35, 295–315, 2000.
Olson, J. R., Crawford, J. H., Davis, D. D., Chen, G., Avery, M. A., Barrick, J. D. W., Sachse, G. W., Vay, S. A., Sandholm, S. T., Tan, D., Brune, W. H., Faloona, I. C., Heikes, B. G., Shetter, R. E., Lefer, B. L., Singh, H. B., Talbot, R. W., and Blake, D. R.: Seasonal differences in the photochemistry of the South Pacific: a comparison of observations and model results from PEM-Tropics A and B, J. Geophys. Res., 106, 32749–32766, 2001.

ACPD
10, 22219–22277, 2010

Olson, J. R., Crawford, J. H., Chen, G., Brune, W. H., Faloona, I. C., Tan, D., Harder, H., and Martinez, M.: A reevaluation of airborne HO_x observations from NASA field campaigns, J. Geophys. Res., 111, D10301, doi:10.1029/2005JD006617, 2006.

Orlando, J. J., Tyndall, G. S., Apel, E. C., Riemer, D. D., and Paulson, S. E.: Rate coefficients and mechanisms of the reaction of Cl-atoms with a series of unsaturated hydrocarbons under atmospheric conditions, Int. J. Chem. Kinet., 35, 334–353, 2003.

Ren, X. R., Brune, W. H., Cantrell, C. A., Edwards, G. D., Shirley, T., Metcalf, A. R., and Lesher, R. L.: Hydroxyl and peroxy radical chemistry in a rural area of Central Pennsylvania: Observations and model comparisons, J. Atmos. Chem., 52, 231–257, doi:10.1007/s10874-005-3651-7, 2005.

Ren, X., Brune, W. H., Mao, J., Mitchell, M. J., Lesher, R. L., Simpas, J. B., Metcalf, A. R., Schwab, J. J., Cai, C., Li, Y., Demerjian, K. L., Felton, H. D., Boynton, G., Adams, A., Perry, J., He, Y., Zhou, X., and Hou, J.: Behavior of OH and HO_2 in the winter atmosphere in New York city, Atmos. Environ., 40, S252–S263, doi:10.1016/j.atmosenv.2005.11.073, 2006.

Ridley, B., Ott, L., Pickering, K., Emmons, L., Montzka, D., Weinheimer, A., Knapp, D., Grahek, F., Li, L., Heymsfield, G., McGill, M., Kucera, P., Mahoney, M. J., Baumgardner, D., Schultz, M., and Brasseur, G.: Florida thunderstorms: a faucet of reactive nitrogen to the upper troposphere, J. Geophys. Res., 109, D17305, doi:10.1029/2004JD004769, 2004.

Sander, S. P. and Watson, R. T.: A Kinetics study of the reaction of SO_2 with CH_3O_2, Chem. Phys. Lett., 77, 473–475, 1981.

Sander, S. P., Friedl, R. R., Golden, D. M., Kurylo, M. J., Moortgat, G. K., Wine, P. H., Ravishankara, A. R., Kolb, C. E., Molina, M. J., Finlayson-Pitts, B. J., Huie, R. E., and Orkin, V. L.: Chemical Kinetics and Photochemical Data for Use in Atmospheric Studies Evaluation Number 15, NASA Jet Propulsion Laboratory, 2006.

Singh, H. B., Brune, W. H., Crawford, J. H., Flocke, F., and Jacob, D. J.: Chemistry and transport of pollution over the Gulf of Mexico and the Pacific: spring 2006 INTEX-B campaign overview and first results, Atmos. Chem. Phys., 9, 2301–2318, doi:10.5194/acp-9-2301-2009, 2009.

Suh, I., Zhang, R. Y., Molina, L. T., and Molina, M. J.: Oxidation mechanism of aromatic peroxy and bicyclic radicals from OH-toluene reactions, J. Am. Chem. Soc., 125, 12655–12665, 2003.

Taatjes, C. A.: Time-resolved infrared absorption measurements of product formation in Cl atom reactions with alkenes and alkynes, Int. Rev. Phys. Chem., 18, 419–458, 1999.

ACPD
10, 22219–22277, 2010

Tanner, D. J. and Eisele, F. L.: Present OH measurement limits and associated uncertainties, J. Geophys. Res., 100, 2883–2892, 1995.

Tully, F. P., Goldsmith, J. E. M., and Droege, A. T.: Hydrogen-atom abstraction from alkanes by OH .4. Isobutane, J. Phys. Chem., 90, 5932–5937, 1986.

Tyndall, G. S., Cox, R. A., Granier, C., Lesclaux, R., Moortgat, G. K., Pilling, M. J., Ravishankara, A. R., and Wallington, T. J.: Atmospheric chemistry of small organic peroxy radicals, J. Geophys. Res., 106, 12157–12182, 2001.

ACPD

10, 22219–22277, 2010

Table 1. Standard Ambient PeRCIMS Operating Conditions.

Mode	HO_2+RO_2	HO_2
Diluent	O_2	N_2
Sampled Air:Diluent	1:1	1:1
Inlet NO mixing ratio	15.0 ppmv	67.5 ppmv
Inlet SO_2 mixing ratio	400 ppmv	1800 ppmv
O_2 mixing ratio	58.0%	10.1%
Inlet [NO]/[O_2]	2.53×10^{-5}	6.80×10^{-4}
$\alpha_{CH_3O_2}$	1.22 ± 0.08	0.17 ± 0.04
$\Delta[H_2SO_4]/[HO_2]_o$ yield	5.5	5.5
Reaction time (neutral region)	0.124 s (101 kPa); 0.276 s (50.5 kPa)	
Reaction time (ion region)	0.276 s (101 kPa); 0.552 s (50.5 kPa)	
Inlet pressure	Variable, but typically held at 2×10^4 Pa	
Chamber pressure	Differentially pumped, from 1.0 to $< 1.0 \times 10^3$ Pa	
Detection method	Quadrupole mass spectrometry of HSO_4^-	
Detection limit	2 pptv	
Electronic noise	<1% of radical signal	
Signal/background ratio	>2:1 for most ambient conditions	

ACPD
10, 22219–22277, 2010

Table 2. Summary of the mean $\alpha_{CH_3O_2}$ values from methane experiments according to inlet [NO]/[O_2].

Inlet [NO]/[O_2] Range		Mean $\alpha_{CH_3O_2}$ [a]	Number of Measurements[b]
$(2.21–4.42) \times 10^{-3}$		0.09	1
$(1.10–2.21) \times 10^{-3}$		0.09 ± 0.03	22
$(0.55–1.10) \times 10^{-3}$		0.16 ± 0.04	230
$(2.76–5.52) \times 10^{-4}$		0.22 ± 0.04	70
$(1.38–2.76) \times 10^{-4}$		0.36 ± 0.06	51
$(0.69–1.38) \times 10^{-4}$		0.62 ± 0.07	31
$(3.45–6.91) \times 10^{-5}$		0.88 ± 0.11	64
$(1.73–3.45) \times 10^{-5}$		1.19 ± 0.11	370
$(0.86–1.73) \times 10^{-5}$		1.50 ± 0.10	157
$(4.32–8.63) \times 10^{-6}$		1.56 ± 0.11	40
$(2.16–4.32) \times 10^{-6}$		1.70 ± 0.12	44
$(1.08–2.16) \times 10^{-6}$		1.55 ± 0.24	40
Ambient Mode	[NO]/[O_2]		
HO_2	6.80×10^{-4}	0.17 ± 0.04	159
HO_2+RO_2	2.53×10^{-5}	1.22 ± 0.08	159

[a] For [NO]/[O_2] ranges in which more than $\alpha_{CH_3O_2}$ one measurement was made, the uncertainty is the standard error of the mean.
[b] Each $\alpha_{CH_3O_2}$ measurement is determined from the mean of four individual peroxy radical measurements with CH_4 added to the humidified air and the mean of four measurements with H_2 added to the humidified air.

ACPD
10, 22219–22277, 2010

Table 3. Summary of $\alpha_{CH_3O_2}$ dependence on the total flow of humidified air through the calibration cell.

Dry Air, SLPM	Humidified Air, SLPM	Hg Lamp Distance, inches	Slit Width, inches	HO_2 radicals, pptV	Mean $\alpha_{CH_3O_2}$ [a]
1.25	0.125	1.0	0.5	210	2.06 ± 0.02
1.25	0.125	2.0	0.5	139	1.81 ± 0.04
1.25	0.125	4.0	0.5	53	1.69 ± 0.02
1.75	0.175	1.0	0.5	234	1.65 ± 0.02
1.75	0.175	2.0	0.5	111	1.39 ± 0.05
1.75	0.175	4.0	0.5	49	1.36 ± 0.03
2.50	0.250	1.0	0.5	221	1.30 ± 0.02
2.50	0.250	2.0	0.5	123	1.22 ± 0.03
2.50	0.250	4.0	0.5	40	1.21 ± 0.02
3.75	0.375	1.0	0.5	172	1.19 ± 0.02
3.75	0.375	2.0	0.5	90	1.12 ± 0.02
3.75	0.375	4.0	0.5	29	1.10 ± 0.03
5.00	0.500	1.0	0.5	137	1.10 ± 0.03
5.00	0.500	2.0	0.5	68	1.08 ± 0.03
5.00	0.500	4.0	0.5	23	1.14 ± 0.02

[a] Uncertainties are the standard errors of the mean $\alpha_{CH_3O_2}$ values.

ACPD
10, 22219–22277, 2010

Table 4. Dependence of calibration factors and $\alpha_{CH_3O_2}$ values on calibration cell pressure.

Calibration Cell Pressure, mbar	F, $\times 10^3$		$\alpha_{CH_3O_2}$,[a]	
	HO_2+RO_2 mode	HO_2 mode	HO_2+RO_2 mode	HO_2 mode
933	18.2 ± 1.0	14.8 ± 1.0	1.26 ± 0.05 (12)	0.15 ± 0.02 (12)
840	18.3 ± 1.0	14.5 ± 1.0	1.20 ± 0.08 (17)	0.16 ± 0.04 (17)
667	17.6 ± 1.0	15.9 ± 1.0	1.24 ± 0.05 (4)	0.17 ± 0.03 (4)
533	16.8 ± 1.3	17.6 ± 1.0	1.20 ± 0.08 (21)	0.15 ± 0.04 (21)
400	17.7 ± 1.9	16.8 ± 2.2	1.16 ± 0.07 (4)	0.17 ± 0.02 (4)

[a] Mean $\alpha_{CH_3O_2}$ values are shown, with the number of individual $\alpha_{CH_3O_2}$ determinations used in the mean in parentheses. Errors are the standard errors of the means.

ACPD
10, 22219–22277, 2010

Table 5. Summary of mean α_{RO_2} values from studied RO_2 precursors.

RO_2 Precursor	$10^{-12} \times k_{OH}$ [a] (298 K) (cm^3 molecules^{-1} s^{-1})	Mean α_{RO_2} [b]	
		HO_2+RO_2 mode	HO_2 mode
methane	0.00640	1.22 ± 0.08 (159)	0.17 ± 0.04 (159)
ethane	0.248	1.38 ± 0.06 (2)	0.342 ± 0.003 (2)
propane	1.09	1.41 ± 0.04 (6)	0.30 ± 0.03 (6)
n-butane	2.36	1.35 ± 0.03 (2)	0.45 ± 0.05 (2)
methylpropane	2.12	0.33 ± 0.03 (27)	0.03 ± 0.01 (4)
n-pentane	3.80	1.41 ± 0.05 (8)	0.89 ± 0.02 (9)
methylbutane	3.6	1.40 ± 0.06 (4)	0.36 ± 0.02 (4)
n-hexane	5.20	1.20 ± 0.03 (3)	1.03 ± 0.01 (4)
2-methylpentane	5.2	1.18 ± 0.02 (3)	0.77 ± 0.04 (4)
3-methylpentane	5.2	0.94 ± 0.23 (6)	0.28 ± 0.06 (6)
cyclohexane	6.97	1.04 ± 0.04 (7)	0.70 ± 0.04 (8)
n-heptane	6.76	1.05 ± 0.02 (4)	0.95 ± 0.02 (5)
ethene	8.52	1.45 ± 0.07 (7)	1.11 ± 0.05 (7)
propene	26.3	1.65 ± 0.02 (3)	1.37 ± 0.03 (4)
1-butene	31.4	1.52 ± 0.02 (3)	1.15 ± 0.02 (4)
isoprene	100	1.18 ± 0.05 (4)	1.12 ± 0.03 (4)
benzene	1.22	0.94 ± 0.05 (3)	0.89 ± 0.03 (3)
toluene	5.63	0.89 ± 0.04 (8)	0.75 ± 0.03 (8)

[a] From Atkinson and Arey (2003).

[b] Uncertainties are the standard errors in the mean α_{RO_2} for values measured at inlet [NO]/[O_2] ratios within ±15% of the HO_2 and HO_2 + RO_2 modes (see Table 1). Numbers in parentheses are the numbers of individual α_{RO_2} values used to determine the means.

ACPD
10, 22219–22277, 2010

Table 6. Parameterized box model RO_2 groups comprising the non-CH_3O_2 RO_2.

RO_2 group	Product of Reaction	RO_2 structure	RO_2 measured?
ETO2	ethane + OH	$C_2H_5O_2$	yes
n-R3O2	propane + OH	*n*-$C_3H_7O_2$	yes
i-R3O2	propane + OH	*i*-$C_3H_7O_2$	yes
RAO2	lumped C_4+ alkanes + OH	various $C_nH_{2n+1}O_2$	partial
EO2	ethene + OH	$HOCH_2CH_2O_2$	as HO_2
PO2	propene + OH	$HOC_3H_6O_2$	as HO_2
CHO2	lumped alkenes + O_3	various	as HO_2
CRO2	lumped alkenes + O_3	various	as HO_2
PRN1	lumped alkenes + NO_3	various	partial
ADDB	benzene + OH	$C_6H_6(OH)O_2$	as HO_2
TO2	C_7+ aromatics + OH	various	partial
RIO2	isoprene + OH	various	as HO_2
VRO2	MVK + OH	various	as HO_2
MRO2	methacrolein + OH	methacrolein RO_2	as HO_2
INO2	isoprene + NO_3	various	as HO_2
ISOPO2	lumped isoprene products + OH	various	as HO_2
ATO2	acetone + OH	$CH_3COCH_2O_2$	yes
KO2	MEK (methyl ethyl ketone) + OH	MEK RO_2	very likely
MCO3	various	CH_3CO_3	yes
RCO3	associated with PPN ($C_2H_5CO_3NO_2$)	various	as HO_2
TCO3	decomposition of $CHOCH=CHCO_3NO_2$	$CHOCH=CH_3O_3$	partial
ZO2	lumped aromatic RO_2	various	partial
MAO3	decomposition of MPAN (from methacrolein)	$CH_2=C(CH_3)CO_3$	as HO_2
RAN1	lumped C_4 + alkyl nitrates + OH	various	as HO_2
RANO2	lumped RAN1 + NO	various	as HO_2

ACPD
10, 22219–22277, 2010

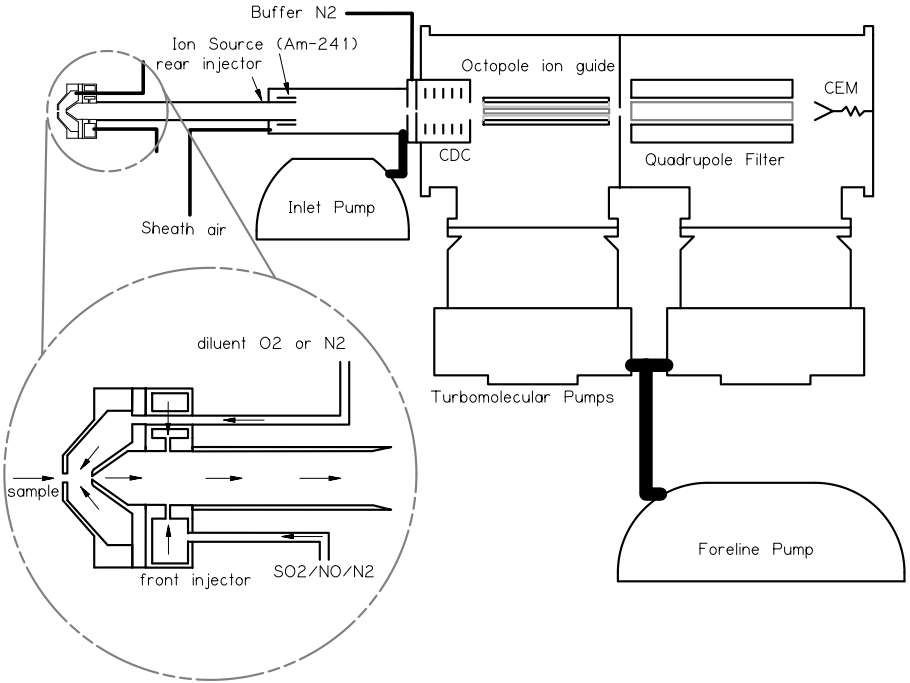

Fig. 1. Schematic of PeRCIMS instrument, with inset of modified inlet and dilution region.

ACPD
10, 22219–22277, 2010

CIMS Measurements of HO_2 and RO_2

R. S. Hornbrook et al.

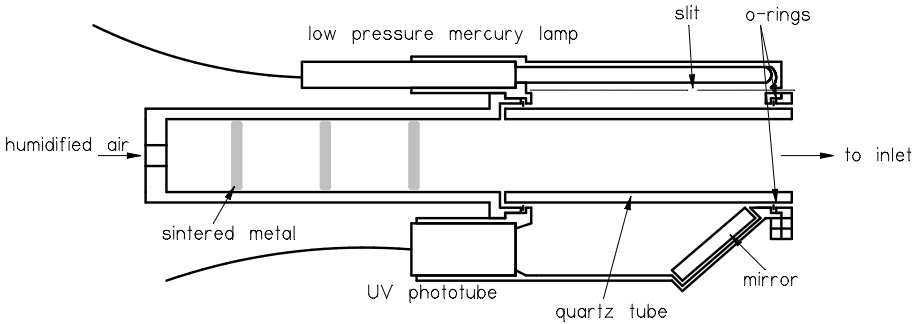

Fig. 2. Schematic of new calibration cell.

ACPD
10, 22219–22277, 2010

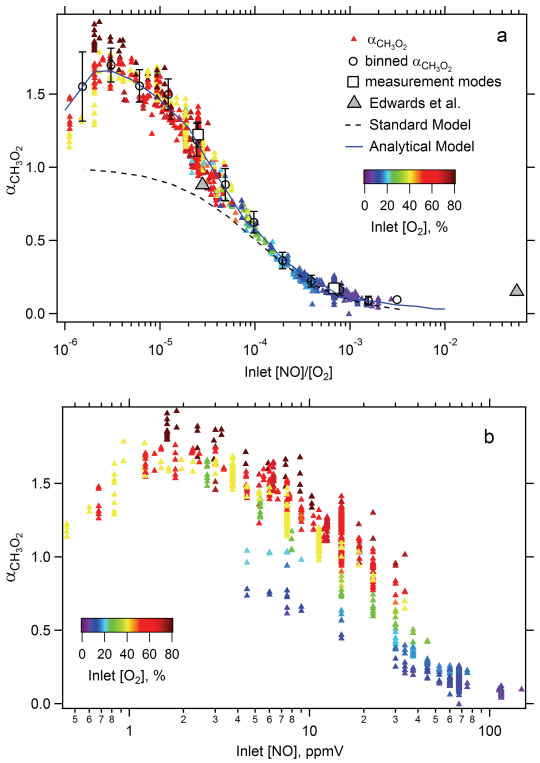

Fig. 3. Plot of measured $\alpha_{CH_3O_2}$ against **(a)** the ratio of [NO]/[O_2] in the inlet and **(b)** inlet [NO]. Individual measurements are shown as small triangles, colored according to inlet O_2 concentration. In (a) the open black circles are the average measured $\alpha_{CH_3O_2}$ values binned by [NO]/[O_2], with error bars showing the standard deviation for each bin. Squares are the mean $\alpha_{CH_3O_2}$ values for the two ambient measurement modes. Large grey triangles are the literature $\alpha_{CH_3O_2}$ values reported by Edwards et al. (2003). Also shown are the standard model (dashed curve) and the analytical model (solid blue curve) fit to the results.

ACPD
10, 22219–22277, 2010

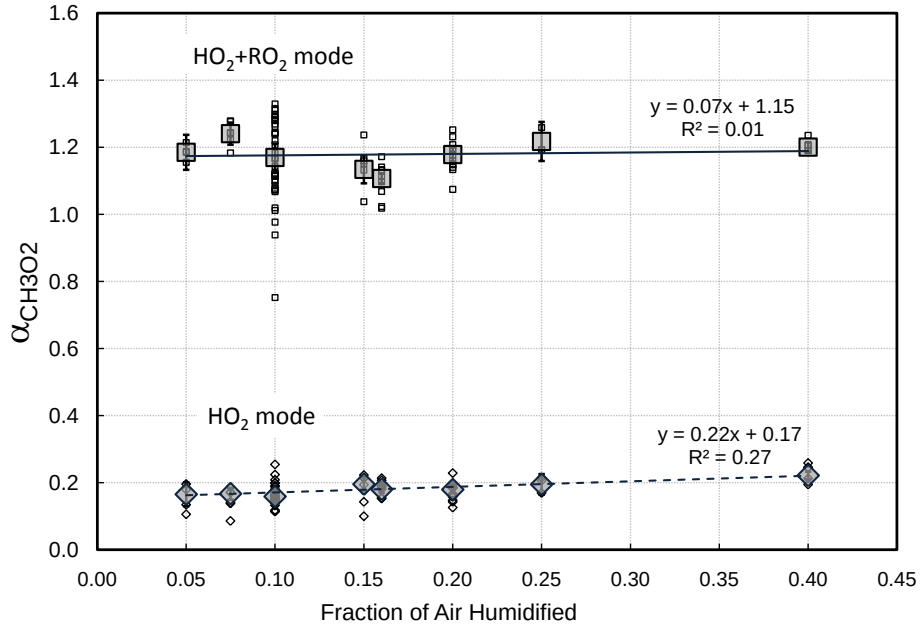

Fig. 4. Dependence of $\alpha_{CH_3O_2}$ on the fraction of calibrator air that has been saturated for the $HO_2 + RO_2$ and HO_2 modes. Smaller points show individual $\alpha_{CH_3O_2}$ measurements, and larger points are the error-weighted means of the $\alpha_{CH_3O_2}$ determinations at each humidity. Error bars show the error-weighted standard errors.

ACPD
10, 22219–22277, 2010

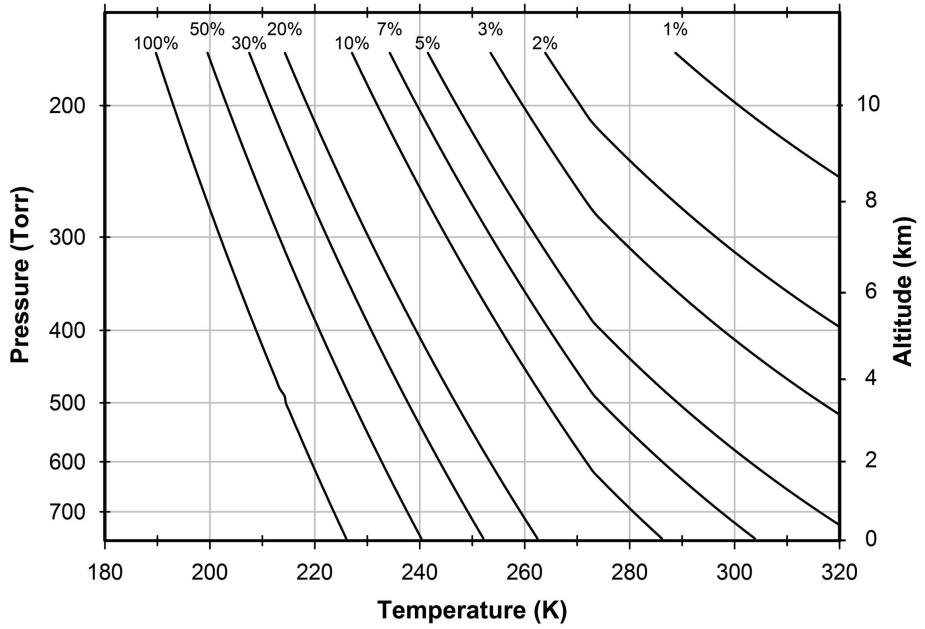

Fig. 5. The basic operating region for the PeRCIMS inlet: the curves show the calculated dependence on ambient pressure/altitude and temperature for a series of minimum ambient relative humidities. Below the curves, modifications to increase water vapor in the inlet region are required to maintain measurement sensitivity.

ACPD
10, 22219–22277, 2010

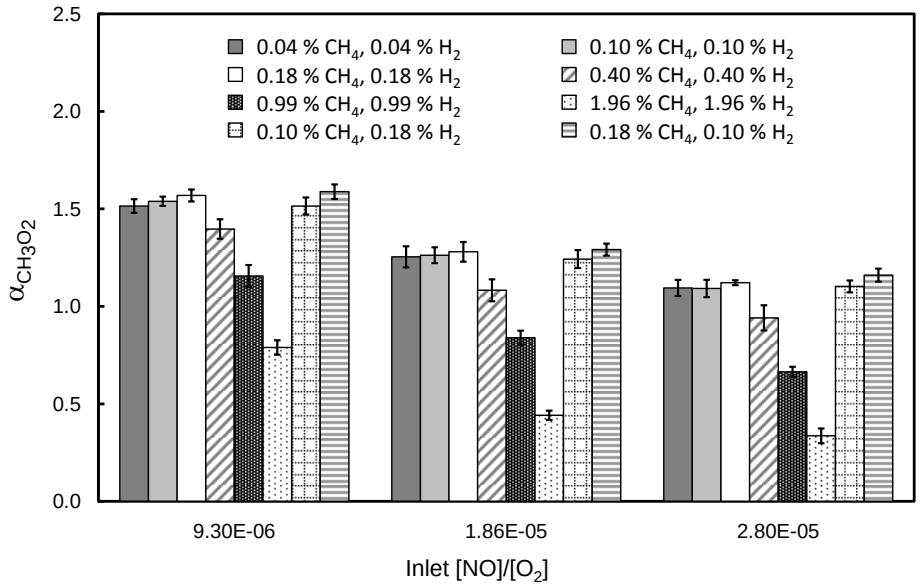

Fig. 6. Dependence of $\alpha_{CH_3O_2}$ on the H_2 and CH_4 mixing ratios in the calibration cell air mixture at three inlet [NO]/[O_2] conditions. Error bars show the standard error of each $\alpha_{CH_3O_2}$ determination.

ACPD
10, 22219–22277, 2010

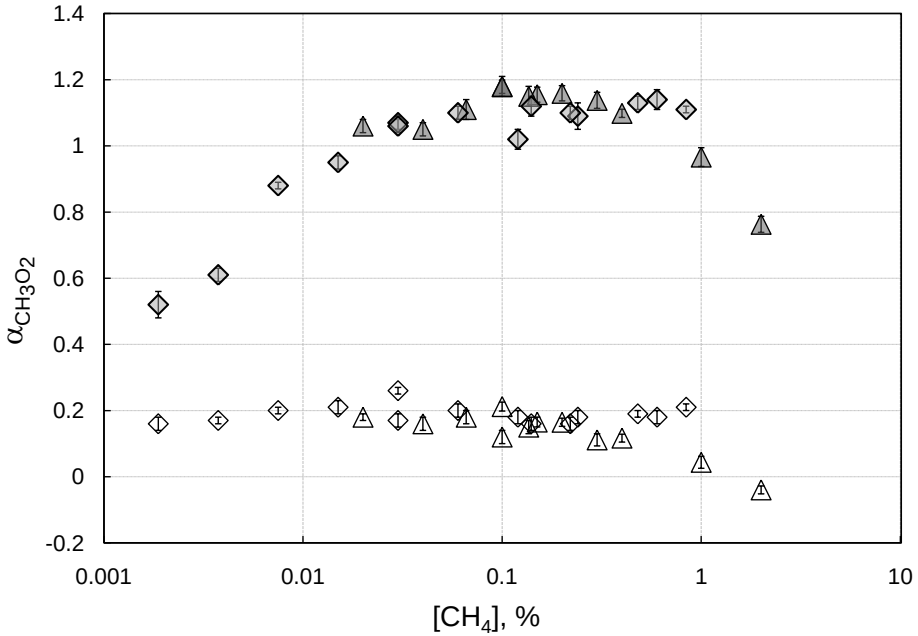

Fig. 7. Dependence of $\alpha_{CH_3O_2}$ on CH_4 mixing ratio in the calibration cell. Closed and open symbols are the measured $\alpha_{CH_3O_2}$ values at the $HO_2 + RO_2$ mode and HO_2 mode, respectively, and triangles and diamonds are the results from the single-dilution and double-dilution measurements, respectively. Error bars show the standard errors of each $\alpha_{CH_3O_2}$ determination.

ACPD
10, 22219–22277, 2010

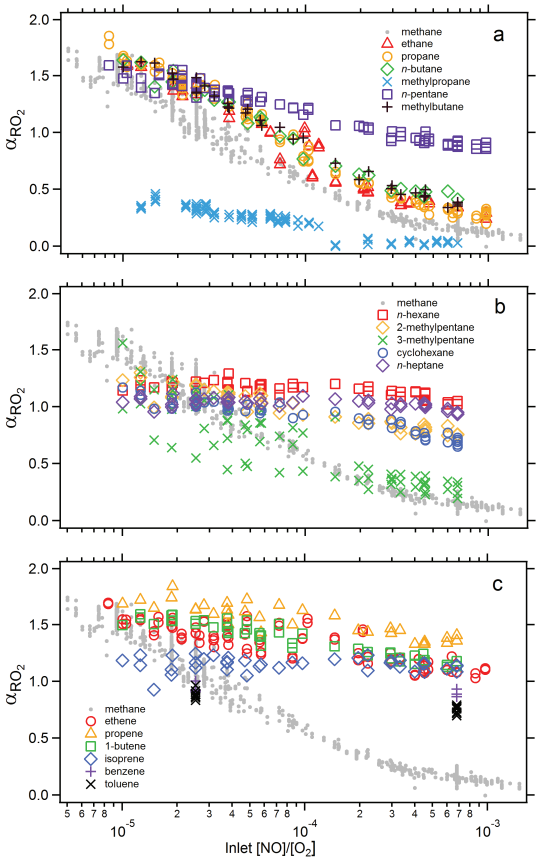

Fig. 8. Plots of α_{RO_2} for RO_2 formed from **(a)** C_2-C_5 (i.e. having between two and five carbon atoms) alkane precursors **(b)** C_6-C_7 alkane precursors and **(c)** unsaturated hydrocarbon precursors against the ratio of $[NO]/[O_2]$ in the inlet. For comparison, measured $\alpha_{CH_3O_2}$ values are included on each plot.

ACPD
10, 22219–22277, 2010

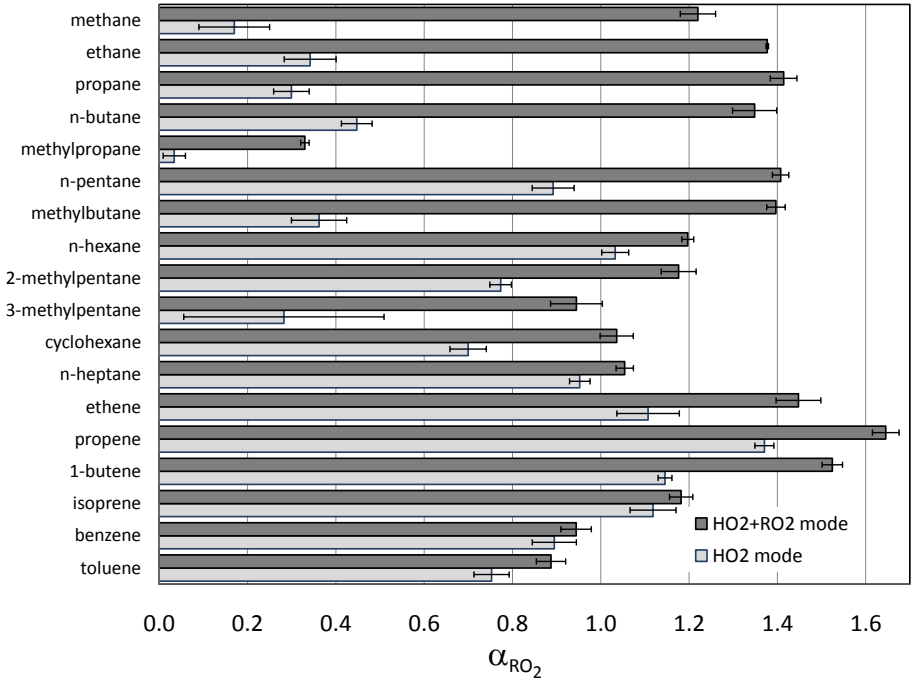

Fig. 9. Comparison of measured mean α_{RO_2} for a number of RO_2 precursors at the $HO_2 + RO_2$ and HO_2 measurement modes (i.e. $[NO]/[O_2] = 2.53 \times 10^{-5}$ and 6.80×10^{-4}, respectively.) Error bars show the standard errors of the α_{RO_2} measurements for each precursor made within ±15% of the above $[NO]/[O_2]$ for each measurement mode.

ACPD
10, 22219–22277, 2010

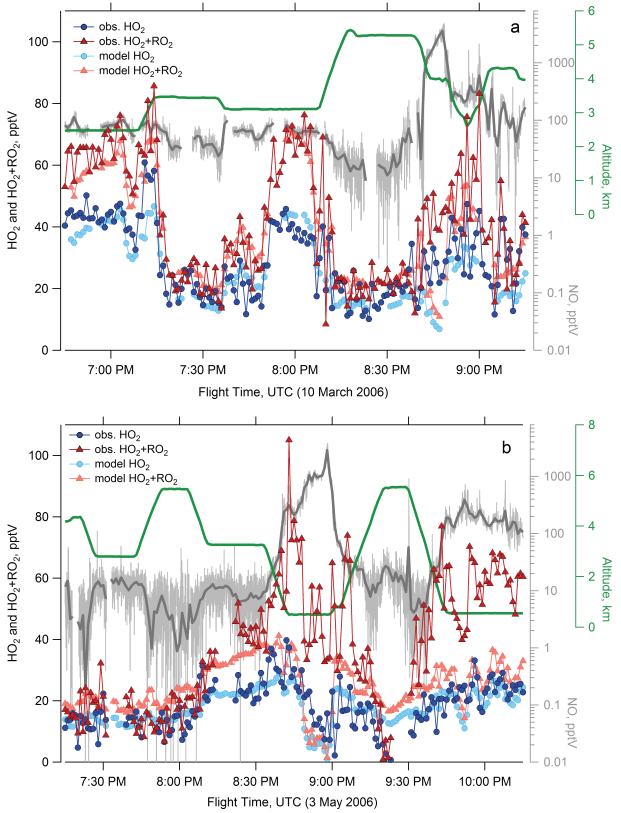

Fig. 10. Time-series plots of observed and modeled peroxy radical mixing ratios for the C-130 flights on **(a)** 10 March 2006 and **(b)** 3 May 2006. In both, the altitude profile is the solid green trace, 1-Hz [NO] observations are shown in light grey, and the 1-min averaged [NO] is shown in dark grey.

ACPD
10, 22219–22277, 2010

CIMS Measurements of HO_2 and RO_2

R. S. Hornbrook et al.

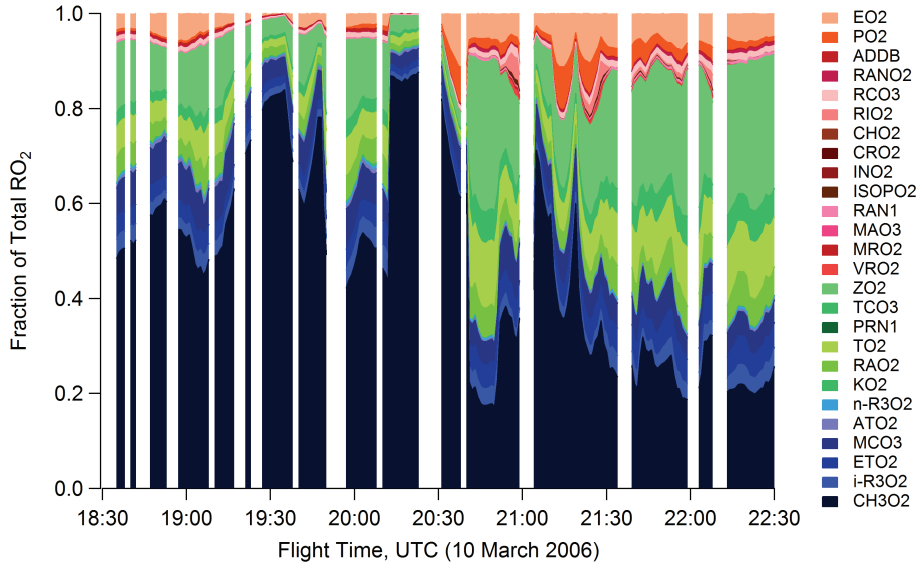

Fig. 11. Time-series plot of modeled RO_2 groups as a fraction of the total RO_2 for the flight on 10 March 2006. Blue-toned groups are those that are primarily measured in the $HO_2 + RO_2$ mode and not in the HO_2 mode, red-toned groups are those that are likely measured in the HO_2 mode, and green-toned groups are those that contain a mixture of RO_2 that generate signals in the HO_2 and the $HO_2 + RO_2$ modes. A full description of the RO_2 groups is in Table 6.

ACPD
10, 22219–22277, 2010

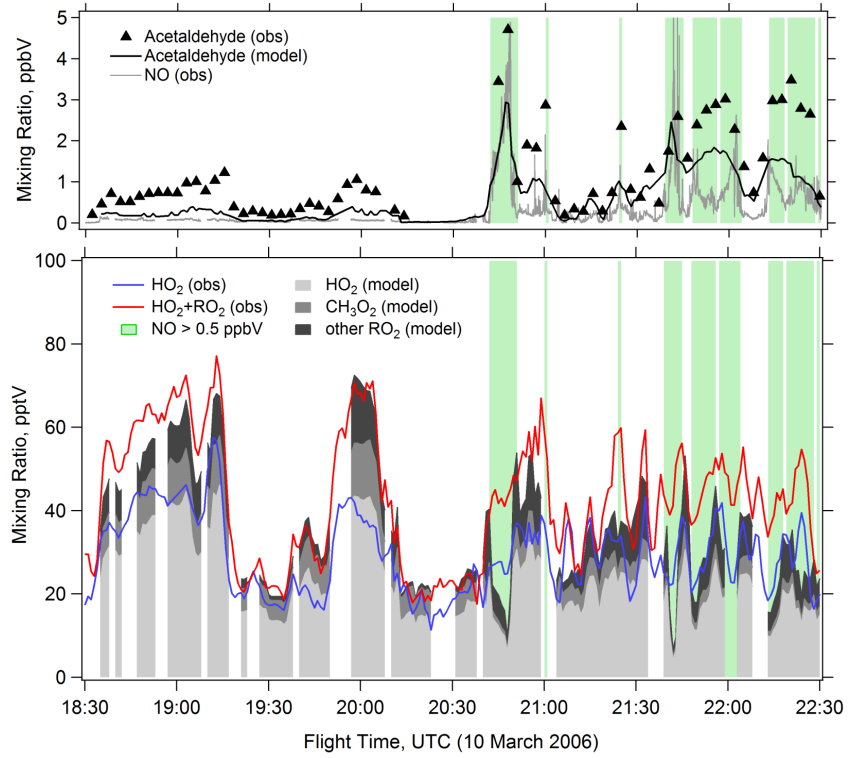

Fig. 12. Time-series plot of the observed and modeled acetaldehyde (top panel) and peroxy radicals (bottom panel) during a section of the flight on 10 March 2006. The stacked grey areas show the modeled [HO_2], [CH_3O_2] and non-CH_3O_2 [RO_2]. The blue and red lines show the observed [HO_2] and [$HO_2 + RO_2$], respectively. The 1-s [NO] is shown in grey (top panel), and time periods when the 1-min average of the observed [NO] is greater than 0.5 ppbV are highlighted in green.

ACPD
10, 22219–22277, 2010

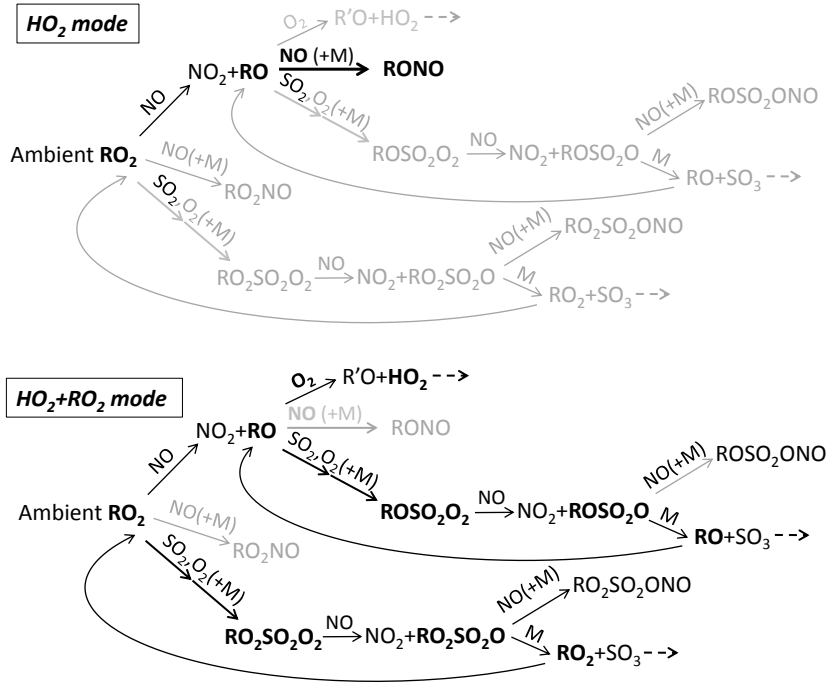

Scheme 1. Inlet RO_2 chemistry.

ACPD
10, 22219–22277, 2010

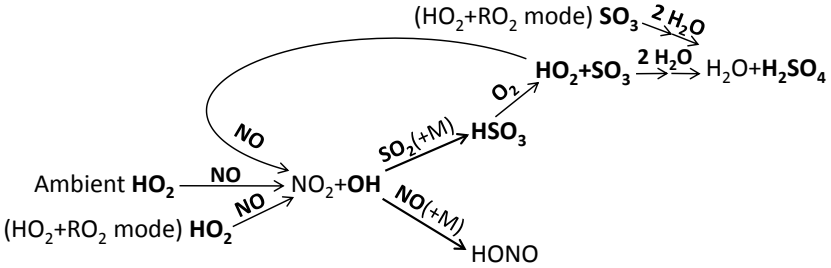

Scheme 2. Inlet HO_2 chemistry.

ACPD
10, 22219–22277, 2010